LUND UNIVERSITY
Faculty of Science

Investigation of phase conjugation for medical imaging

Ivan Sytcevich

Thesis submitted for the degree of Master of Science
Project duration: 9 months

Supervised by Stefan Kröll and Qian Li

Department of Physics
Division of Atomic Physics
May 2017

Abstract

With the development of extremely precise spectral filters based on spectral hole burning and slow light effects, the idea of their implementation in an Ultrasound Optical Tomography (UOT) medical imaging technique arose. Simulations have shown that the resulting Contrast-to-Noise Ratio (CNR) is fairly good at depths up to 5 cm but decreases dramatically when probing deeper in tissue. One of the possible enhancements of this technique is to include a phase conjugator after the filter to reverse and amplify ultrasound-tagged photons and send them back to the area of interest. This project tries to investigate the possibilities of using rare-earth-ion-doped crystals as possible phase-conjugating elements in the UOT and is specifically aimed at studying the properties of an optical phase conjugation process in these media. Experimental work was done on two crystals doped with Praseodymium, and the phase-conjugated signal was investigated as a function of different parameters with results discussed and presented in the respective section. In particular, efficient phase conjugation was observed in a 6-mm thick Pr^{3+}:Y_2SiO_5 crystal with reflectivity values reaching up to 124 %. Further outlook and possible applications are given at the end of the thesis.

Popular Science Summary

Despite being extremely useful in all areas of modern medicine, laser still faces a challenging obstacle when used as a diagnostics and imaging tool. Its radiation is heavily affected by tissue, i.e. light can not get deep enough in the medium without being weakened and distorted. The reason for this attenuation and distortion is two processes that happen when light propagates inside the body - absorption (the light energy is absorbed by molecules and atoms in the medium) and scattering (light randomly changes the direction of propagation due to interaction with atoms and molecules).

While little can be done to reduce the light absorption in tissue, in principle, there are certain ways that can remove the effect of scattering. One of those tricks is a process of Optical Phase Conjugation. It is an effect where one combines three laser beams in a medium such that they create a fourth beam that is the exact copy of one of the input beams but with reversed direction of propagation. This is sometimes viewed as a "magic mirror" that reflects the light in such a way that it travels backwards in time. Optical phase conjugation is a highly promising technique with a broad range of applications in modern physics.

This very useful phenomenon can, in theory, be implemented in a medical imaging technique called Ultrasound-mediated Optical Tomography (UOT). In this technique, laser light interacts with a sound wave that is sent into the area that the scientist wants to observe. Ultrasound is generally much more resistant to attenuating properties of tissue and propagates in media like skin and muscles more or less freely (there are some exceptions, though, e.g. - bones). At the same time light and sound can interact with each other, and when this happens, the former gets a wavelength shift (colour change). We can refer to this light as being "tagged" by the ultrasound. By detecting this particular colour-shifted signal, it is possible to get an idea of what is happening in the place where the light and sound interacted with each other. By moving the ultrasound pulse to different spots, people can "map" area that they want to observe and thus get a full image of the region of interest.

Although UOT shows a great deal of promise as a future imaging method, there is a significant amount of engineering obstacles that scientists have to overcome in order to push this technique forward into the medical industry. One of these barriers is the detection of this ultrasound-tagged light. Only a small fraction of incoming light particles is lucky enough to reach the ultrasound focus and get the colour shift, so the total signal from those will be much weaker compared to the intense background light that did not reach the ultrasound. This light not having interacted with the ultrasound should be filtered out. It can be done by using very precise filters which are transparent only in narrow 'wavelength window' constructed for the tagged photons while being opaque to the unshifted background

light. Still, even after filtering, it may be hard to get good contrast and resolution of the target area.

That is where optical phase conjugation comes into play: the general idea is to send back and amplify the tagged light. Phase conjugation removes the randomness of the scattering process out of the equation since the conjugated (reversed) wave is intimately connected to the original wave and will be scattered straight back to the ultrasound focus. The light will be collected on the side of the input and in theory is able to carry more power compared to the signal before the phase conjugation.

The next question is what material should people use for this special mirror? Extensive studies on the phase conjugation in different materials were conducted in recent years, and all of the studied materials have their own advantages and drawbacks, e.g some are effective but slow, while the others are fast but ineffective. An obvious idea that comes to mind is to use the same material for phase conjugation as for the light filtering. Filters described above are based on inorganic crystals doped with rare-earth elements, so in principle, it would be convenient to use them for the phase conjugation as well. The primary goal of this master project is to investigate that possibility and study the properties of the phase conjugation in these structures.

Over the course of last year, experiments were done on two samples of different thickness. Studies on a 6-mm thick sample showed some promising results in terms of efficiency of this process but raised a lot of questions on the nature of the optical phase conjugation effect in these crystals. I have tried to give some answers to those questions in the report. This project is ultimately only a tiny part of a bigger collaboration of people working on the implementation of the UOT, and I hope that the findings of this project will give a push to further research on this issue and will help to achieve the end goal.

Acronyms and Abbreviations

UOT - Ultrasound Optical Tomography

OPC - Optical Phase Conjugation

YSO - Yttrium Orthosilicate

AOM - acousto-optical modulator

AWG - Arbitrary Waveform Generator

Pr - Praseodymium

Nd - Neodymium

CW - Continuous Wave

DFWM - Degenerate Four-Wave Mixing

RE - Rare-Earth

BWP(FWP) - Backward (Forward) Pump

PC - Phase Conjugation

CNR - Contrast-to-Noise Ratio

FWM - Four-Wave Mixing

US - Ultrasound

BS - Beam splitter

Contents

1 Introduction **1**

2 Theory **3**
2.1 Optical phase conjugation 3
2.2 OPC in rare-earth-ion-doped solids 5
2.3 Ultrasound Optical Tomography 7

3 Experimental methods, setup and equipment **10**
3.1 Praseodymium-doped crystals 10
3.2 Spectral Hole Burning 11
3.3 Laser system and optical setup 12
3.4 Beam overlap 13

4 Results and discussion (1 mm crystal) **16**
4.1 Signal structure. Efficiency 16
4.2 Absorption 17
4.3 Pulse Duration 18
4.4 Rabi frequency. Incoming beam intensity 19
4.5 Slow light experiments 22

5 Results and discussion (6 mm crystal) **25**
5.1 Signal structure 25
5.2 Chirp rate 26
5.3 Pulse duration 28
5.4 Rabi frequency. Beam Intensity 30
5.5 Polarization. Efficiency 33
5.6 Additional measurements 40

6 Conclusions and Outlook **44**

Acknowledgements **46**

Bibliography **47**

Chapter 1

Introduction

Nowadays laser irradiation in medicine is a vast, rapidly developing research field and a versatile therapeutic tool in treatment, with applications ranging from tumour destruction in oncology to eye surgeries and cosmetic operations like tattoo removal [1–4]. Usage of lasers as a diagnostics and imaging tool is also very promising due to the great contrast it provides, allowing to obtain rich physiological information (i.e. it gives the ability to differentiate between substances on a microscopic level) [5,6]. Another advantage is that the laser light is a non-harmful and safe tool if one operates within standard intensity limits [7,8]. However, there are challenging obstacles that restrict usage of lasers as an imaging technique instrument. Firstly, light is strongly absorbed in human tissue, with absorption coefficients varying strongly as a function of the wavelength. In the majority of cases people tend to work in a "tissue optical window", range of wavelengths roughly from 650 to 900 nm, where absorption is at the lowest for most types of tissue [9]. Secondly, light is scattered by the medium with scattering coefficients varying from 10 to 60 cm^{-1} [10]. Overall, this means that laser radiation is heavily attenuated by the tissue and optical intensities can drop by a large margin as penetration depth increases.

Thus, to get an acceptable signal-to-noise ratio from a designated area, it would be beneficial to overcome at least one of these processes. In theory, scattering can be dealt with by including a phase conjugator in the setup. This device would employ a nonlinear optical effect - phase conjugation by e.g. degenerate four-wave mixing. Phase conjugation is a special geometrical case of degenerate four-wave mixing (DFWM), where three waves create a fourth one which has reversed both the direction of propagation and overall phase factor of the probe (one of the waves participating in the mixing) [11]. PC has been reported to have a great potential in such fields of physics as wavefront (aberration) correction, signal processing and amplification [12]. With a conjugated wave back-tracing the path of the probe, it is possible to get rid of random scattering effects induced by the medium since the scattering will no more govern the path of the light that is coming back (as the conjugate wave has its phase 'bound' to the probe phase). Moreover, the conjugate signal is able to carry more power than the probe since its electric field depends on the amplitudes of supporting waves, the pumps. The basic treatment of the phase conjugation process in transparent media is discussed in more detail in section 2.1. In this project, the role of phase-conjugating mirror is carried out by Yttrium Orthosilicate crystals (YSO) doped with rare-earth Praseodymium ions

(Pr^{3+}). It should be noted that origin and mechanism of optical phase conjugation in such type of material is rather delicate and complex. The discussion in Section 2.2 addresses the studies done earlier on features of PC in rare-earth-ion-doped crystals and solids.

One of the techniques that rely on overcoming the randomness of scattering is ultrasound-mediated optical tomography (UOT). It is an imaging method that employs interaction between an incoming laser field and an ultrasound wave (acousto-optical effect). After such an interaction, the light will obtain a frequency shift equal to the frequency of the ultrasound [13]. In comparison to an optical field, ultrasound is weakly scattered by the tissue and thus can be precisely focused into different parts of the medium allowing to obtain good spatial resolution. As a result, it becomes evident that frequency shifted photons (usually referred as "tagged" photons [14]) are coming from the volume occupied by the ultrasound pulse. Phase conjugation can possibly enhance this technique by back-tracing and amplifying this ultrasound-tagged light back to the focus and help improve overall contrast-to-noise ratio (CNR) in the area of interest. More detailed description and some aspects of this technique are provided in Section 2.3.

This master project primarily concerns experimental work aiming to investigate the properties of phase conjugation in Pr^{3+}:Y_2SiO_5 crystals and their potential usage as a phase-conjugating element in UOT. Chapter 3 describes technical aspects and features of the experiments done and provides the description of the optical setup, sample properties, equipment and software used in the project. Results are presented and discussed in chapters 4 and 5, focused on phase conjugation signal structure, signal efficiency as a function of different parameters (probe and pump beam intensity, detuning of laser frequency from Pr^{3+} ion resonance frequency, etc.); slow light effects and effects of light polarization on the phase-conjugated signal are also considered. Conclusions on the project and further outlook on this topic are given in chapter 6.

Chapter 2

Theory

2.1 Optical phase conjugation

The physical foundation on which this project is based is the process of optical phase conjugation by four-wave mixing (PC-FWM), a nonlinear optical effect that usually originates from the $\chi^{(3)}E^3$ component of polarization density P, where $\chi^{(3)}$ is the third order nonlinear electric susceptibility:

$$P = \epsilon_0(\chi^{(1)}E + \chi^{(2)}E^2 + \chi^{(3)}E^3) \tag{2.1}$$

First, consider the response of the lossless non-amplifying media to three incoming electric fields of frequencies ω_1, ω_2 and ω_3. The total field could be written in the following way:

$$E(t) = \sum_{q=\pm1,\pm2,\pm3} \frac{1}{2}E(\omega_q)\exp(j\omega_q t) \tag{2.2}$$

Where $\omega_{-q} = -\omega_q$, $E(\omega_{-q}) = E^*(\omega_q)$ [13]. This field in general will produce 216 terms in polarization density.

$$P(t) = \frac{1}{8}\chi^{(3)} \sum_{q,r,l=\pm1,\pm2,\pm3} E(\omega_q)E(\omega_r)E(\omega_l)\exp(j(\omega_q + \omega_r + \omega_l)t) \tag{2.3}$$

In order for the waves to successfully mix they should be phase and frequency matched:

$$\omega_1 + \omega_2 = \omega_3 + \omega_4 \tag{2.4}$$

$$\boldsymbol{k_1} + \boldsymbol{k_2} = \boldsymbol{k_3} + \boldsymbol{k_4} \tag{2.5}$$

The phase matching condition is essential for every nonlinear effect and can be understood as conservation of momentum (analogically, frequency matching can be viewed as conservation of energy). The expression for the polarization density for one of the waves that satisfies these conditions would look like:

$$P(\omega_2) = 6\chi^{(3)}E(\omega_3)E(\omega_4)E^*(\omega_1) \tag{2.6}$$

Expressions for other waves look similar.
Consider the case where all of four fields have the same frequency ω, a process

usually named *degenerate four-wave mixing* [13]. If two of four waves have the same complex envelope (e.g. plane, paraboloidal or Gaussian beam profile) and are travelling in the opposite direction, $\boldsymbol{k_4} = -\boldsymbol{k_3}$, then Eq. 2.6 becomes:

$$P(\omega_2) = 6\chi^{(3)}E(\omega_3)E(\omega_4)E^*(\omega_1) = \\ = 6\chi^{(3)}A_3\exp(-i\boldsymbol{k_3}\boldsymbol{r})A_4\exp(-i\boldsymbol{k_4}\boldsymbol{r})E_1^*(\boldsymbol{r}) = A_3A_4E_1^*(\boldsymbol{r}) \quad (2.7)$$

Here, A_3 and A_4 are the amplitudes of the waves 3 and 4. This term of polarization density would correspond to an optical source emitting a wave 2 with complex amplitude E_2:

$$E_2(\boldsymbol{r}) = A_2\exp(-i\boldsymbol{k_2}\boldsymbol{r}) \propto A_3A_4E_1^*(\boldsymbol{r}) = A_3A_4A_1\exp(i\boldsymbol{k_1}\boldsymbol{r}) \quad (2.8)$$

Thus, $\boldsymbol{k_2} = -\boldsymbol{k_1}$ and the nonlinear medium acts like a *phase conjugator*. An intuitive explanation of this effect is that three waves produce fourth wave which is a "time-reversed version" (usually labeled as *signal* or *conjugate*) of one of them, usually named *the probe*, which means that fourth wave is retracing the probe backwards in time, travelling in the opposite direction thus back-tracing the path of the probe. The other two waves that help satisfy phase matching condition are called *the pumps*. Schematic picture of the phase conjugation process is illustrated in Figure 2.1

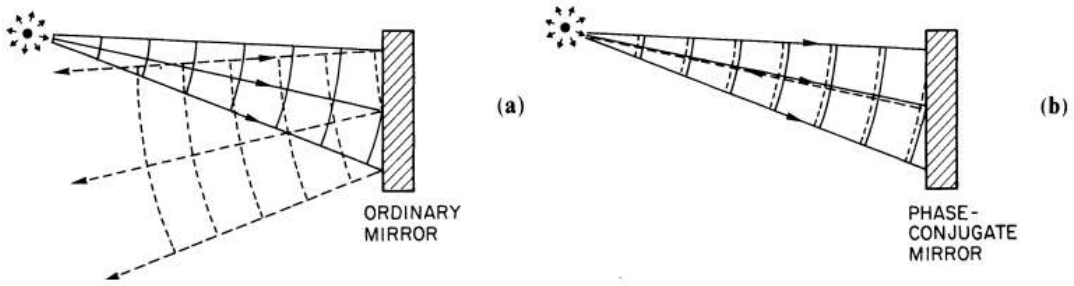

Figure 2.1: Schematic picture of phase conjugation process (a) - Reflection from ordinary mirror, (b) - reflection from phase-conjugating mirror. Figure from [15].

The process of phase conjugation carries a few interesting features. Firstly, the fact that conjugated beam retraces the path of the probe can help remove distortions caused by propagation in external media (optical components in the setup or the sample medium) before the phase conjugator, a feature that is often addressed as *optical reciprocity*. [13, 15] (Figure 2.2).

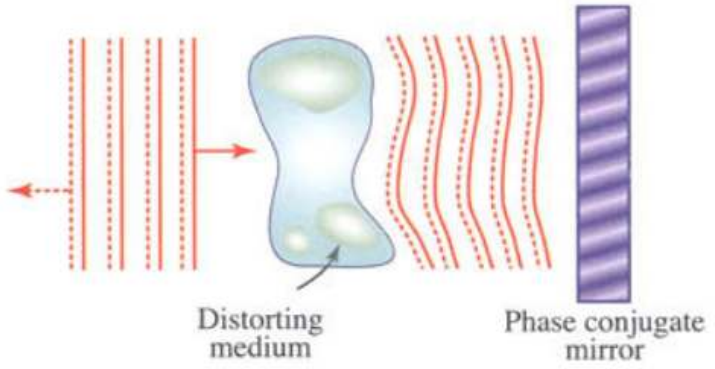

Figure 2.2: Wavefront aberration correction by phase conjugation. Figure from [13].

Moreover, the conjugate wave is able to carry more power than the probe, since its amplitude is proportional to amplitudes of the pump waves. When the intensity of the pumps is sufficiently high, the medium can act like an *amplifying reflector* (reflectivity is larger than unity) [13]. This property can be a valuable asset for numerous applications, including the one investigated in this project.

2.2 OPC in rare-earth-ion-doped solids

There are numerous materials which can possibly be used for PC-FWM. Efficient phase conjugation has been reported in hot and cold gases and vapors (e.g K, Na vapors)[16, 17], liquid crystals and polymers [18, 19], photorefractive crystals and solids [20, 21]. FWM has also been studied in solids doped with a rare-earth (RE) ions [22, 23]. In these structures properties of such doped ions usually play a major role in light-matter interaction and thus optical processes that take place in the crystal. In media, where incoming optical fields have a frequency more or less equal to material's resonance, phase conjugation is often the case of the process of *resonant DFWM* [24]. In the following theoretical discussion, as well as in experiments, the backward DFWM geometry was used (shown on Figure 2.3).

Figure 2.3: Schematic of backward DFWM. Ef,Eb - pumps, Ep,Ec - probe and conjugate [24]

In addition to the approach given in the previous section, another way to describe FWM is to treat it as a Bragg diffraction from an electromagnetically

induced grating. When two laser beams propagate through the sample, they create an interference pattern which modulates the optical properties (complex electric susceptibility) periodically:

$$\Delta\chi = \Delta\chi_0 sin(\Delta\boldsymbol{k}\cdot\boldsymbol{r}) \tag{2.9}$$

In Equation (2.9) $\Delta\boldsymbol{k}$ - wave-vector difference of the beams that create the grating. As can be noted, two counter-propagating pump beams ($\Delta\boldsymbol{k}=0$) do not have any contribution in the creation of the grating that scatters one of the input beams into E_c. Intensity of the scattered conjugate wave is then proportional to $|\Delta\chi_0|^2$ as well as the input intensity of the scattered beam [15, 22]:

$$I_c \propto |\Delta\boldsymbol{\chi_0}|^2 I_b \tag{2.10}$$

Here, I_b is the intensity of the scattered input beam. In general, the parameter $\Delta\chi_0$ in Eqs.(2.9) and (2.10) arises from the fact that electric susceptibilities in ground and excited are different - the interference pattern between two beams creates what is often called a *population grating*. Both real (*dispersive or phase grating*) or imaginary (*absorptive or amplitude grating*) parts of χ usually contribute to the signal, with the absorptive grating dominating the near resonance frequency and the phase grating - far off [15]. To find this change in susceptibility, one often considers the polarization density vector ($\boldsymbol{P}=\chi\epsilon_0\boldsymbol{E}$) in the following form:

$$\boldsymbol{P} = \mathrm{Trace}[\boldsymbol{\mu}\cdot\rho] \tag{2.11}$$

Here $\boldsymbol{\mu}$ is the induced dipole moment and ρ - the density matrix of the system. Components of the density matrix are usually obtained by solving quantum Liuoville's equation (often referred to as Quantum Mechanical Transport Equation [24]):

$$i\hbar(\frac{\partial}{\partial t}+\boldsymbol{v}\cdot\boldsymbol{\nabla})\rho = [H_0,\rho]+[H',\rho]+i\hbar(\frac{dp}{dt})_{\mathrm{sp}} \tag{2.12}$$

Here factor $\boldsymbol{v}\cdot\boldsymbol{\nabla}\rho$ accounts for macroscopic motion of the atoms, H_0 is the initial Hamiltonian of the system, H' is the perturbation caused by applied electromagnetic fields, and last term describes spontaneous decay and relaxation to other states of the system (For solution of Eq.(2.12) in the case of a two-level system see [24])

It should be noted that while knowledge of the density matrix and thus the polarization allows one to obtain an expression for the conjugate wave's electric field (through Maxwell's equations), the question of what is the main factor contributing to the phase conjugate signal remains somewhat controversial (to the authors' knowledge). For the sake of convenience, χ can be expressed in power-series:

$$\chi(E) = \chi^{(1)}+\chi^{(2)}E+\chi^{(3)}E^2 \tag{2.13}$$

Powell *et al.* who worked on DFWM in Nd-doped solids [22] argued that main contribution to the resonant DFWM is due to the grating created by difference in

first-order complex susceptibilities of ground and metastable excited states, $\chi_g^{(1)}$ and $\chi_m^{(1)}$ (while $\chi^{(3)}$ signal is small), so that the first term in Eq. (2.13) becomes:

$$\chi^{(1)} = \chi_g^{(1)} + (\chi_m^{(1)} - \chi_g^{(1)})\frac{N_m}{N} \tag{2.14}$$

Where N_m is the ion concentration in metastable state and N is the total ion concentration.

Ham *et al.* [23] performed phase conjugation experiments on Pr^{3+}:Y_2SiO_5, the same type of crystal as the one investigated in this project. They suppose that the largest part of the signal originates from and is proportional to the parameter $|\chi^{(3)}/Im\chi^{(1)}|$, i.e., third-order susceptibility divided by the absorption. By looking at the mentioned quantity, non-linear effects, in theory, can be enhanced if the absorption coefficient $Im\chi^{(1)}$ is suppressed - this suppression is achieved by a technique called *electromagnetically induced transparency* [25].

To conclude this section, from the available literature it is not obviously clear which mechanism stands as the main driving force for phase conjugation in rare-earth-ion-doped crystals and trying to understand this is one of the tasks being investigated within project's experimental work (Section 4).

2.3 Ultrasound Optical Tomography

Introduced in Chapter 1, Ultrasound Optical Tomography relies on modulation of an incoming laser beam by a focused ultrasound wave. When ultrasound propagates through tissue, it creates a wave-like refractive index distribution (through the introduction of compression and rarefaction zones in the medium [13]). It also causes a displacement of scattering sites which changes the optical path length of light that hit the ultrasound focus. These two effects lead to a phase modulation of an incoming laser beam which in turn leads to the creation of frequency sidebands on either side of the carrier with a separation equal to the frequency of the ultrasound (US). US frequencies of few MHz are usually considered to be used (1-5 MHz) as they provide both good penetration depth and axial resolution [26].

Usually, a very small fraction of photons will be lucky enough to hit the US focus, so the US-modulated signal is very weak compared to large background of unshifted photons, so one of the main challenges of the UOT is to detect and distinguish a weak signal of interest from the strong background light. Various techniques for detection have been proposed, e.g. measuring laser speckle contrast [27], heterodyne parallel speckle detection [28], or using Fabry-Perot cavity to transmit and detect only frequency-shifted component [29]. Jayet *et al.* [30] have proposed a technique that relies on detection of phase conjugated background light with and without presence of ultrasound modulation (frequency shifted photons will no longer participate in PC process due to not meeting frequency and phase matching conditions, so the overall detected signal will decrease).

The detection method that the group at Lund University is primarily concerned with is filtering out background light with precise narrow-band spectral filters [31]. Filtering is achieved by burning a spectral hole in inhomogeneously broadened absorption profile of the filter material (Section 3.2). Tagged photons will have the same frequency as the center of the hole, so the absorption for them will be low, while unshifted light will have frequencies outside the hole and experience strong

absorption and will, therefore, be filtered out. Moreover, light will propagate much slower inside created transmission window owing to creation of steep refractive index distribution which reduces the group velocity of light travelling inside of such window [32, 33] - this will introduce a time delay between shifted and unshifted components. A schematic picture of UOT with slow-light filters is shown in Figure 2.4.

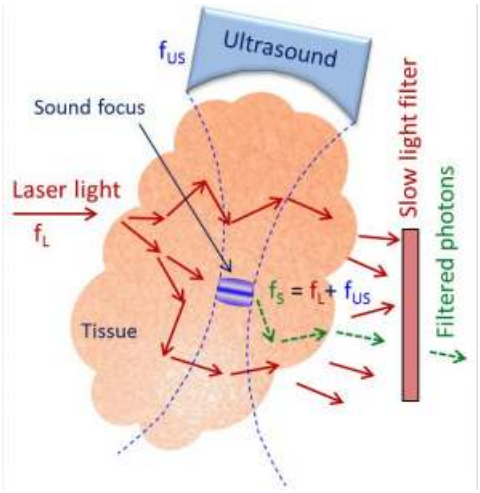

Figure 2.4: Schematic of the UOT principle using slow light filtering [34]. The laser light of frequency f_L is sent through tissue region with an ultrasound pulse of frequency f_{US}. Photons that hit the ultrasound pulse a frequency shift $f_s = f_L + f_{US}$ and propagate through the filter while the background light is filtered out

With these two effects combined, UOT detection using slow light spectral filters shows promising results, with penetration depths reported as deep as 9 cm [35].

As was mentioned before, phase conjugating and amplifying filtered photons can significantly increase signal-to-noise ratio at the ultrasound focus. By placing two elements consisting of filters, gain media and phase conjugators on opposite sides of tissue, it is in theory possible to make a system that transmits light back and forth through an arbitrary point in the tissue (Figure 2.5).

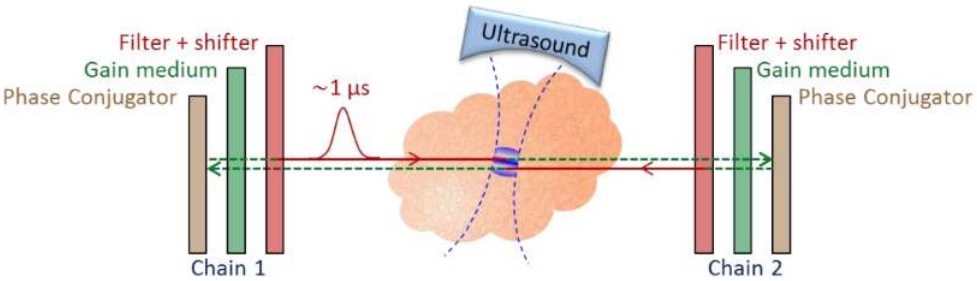

Figure 2.5: Light transmission system through arbitrary point of the body. This system allows one to control the propagation of the laser light inside of the turbid medium by using two chains consisting of three elements: filters transmit the ultrasound-tagged light, phase conjugators reflect it and an external gain media performs the amplification to negate attenuation by absorption. Courtesy of Stefan Kröll

In this setup, to exterminate positive feedback (remove constant iterative frequency shifting by US focus), slow-light filters also function as the frequency

shifters [36], where the frequency shift is achieved by applying external electric field to the crystal (linear Stark Effect) to restore initial light frequency on the way back to the tissue.

Chapter 3

Experimental methods, setup and equipment

3.1 Praseodymium-doped crystals

For this project, two Y_2SiO_5 (YSO) crystals of different length and shape doped with Pr^{3+} ions were used. Doping concentration has a value of 0.05 %. Important parameters of the samples used are presented in the Table 3.1. To avoid birefringence, beams were made to propagate along the optic axis of the crystal (denoted as the b-axis). The orientation of the D1 and D2 principle axes is shown in Figure 3.1. The absorption in an YSO crystal depends on the polarization of incoming light relative to the crystal axes. In the first part of the experiments, all beams had linear polarization orthogonal to the plane of the experimental table (in the 1-mm thick crystal this polarization coincided with the D2 axis, which has the highest absorption coefficient). For the 6-mm thick cylindrical crystal, extensive polarization studies were carried out, where phase conjugation was recorded with different polarizations of incoming beams.

Sample	Dimensions, mm	α at D1, cm^{-1}	α at D2, cm^{-1}
1	5x4x1	3.6± 0.5	47 ± 5
2	12x6	3.6± 0.5	47 ± 5

Table 3.1: Properties of YSO crystals used in the project. The second crystal has a cylindrical shape, and the first dimension is the diameter. Absorption coefficients data from [37]

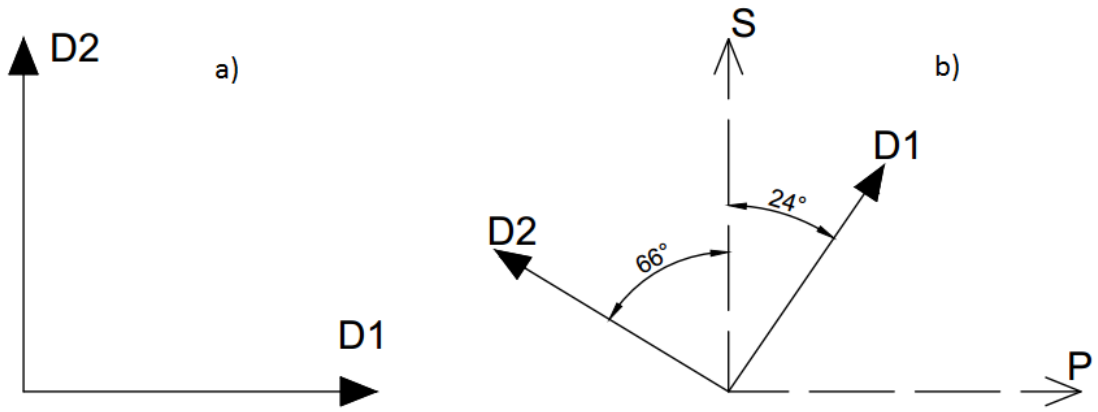

Figure 3.1: Orientation of principle D1 and D2 axes in the samples. a) - 1 mm-thick sample, b) - 6 mm-thick sample. S and P denote orthogonal and parallel polarization, respectively

Samples were mounted on crystal holders (See Figure 3.2) and inserted into the Oxford Instruments Spectromag cryostat. Crystals were cooled down to a temperature of roughly 2.17 K using liquid helium and a Kashiyama NeoDry 15E dry vacuum pump. This was mainly done to prolong coherence times and reduce homogeneous broadening owing to thermal vibrations of the crystal lattice (lattice phonons) [38].

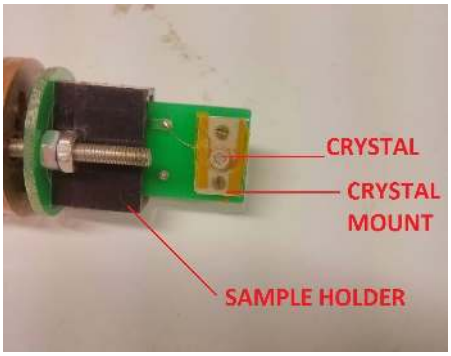

(a) 1-mm thick sample

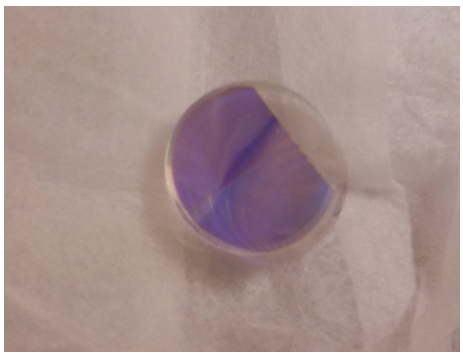

(b) 6-mm thick sample

Figure 3.2: Two Pr^{3+}: Y_2SiO_5 crystals used in the experiments. For the 6-mm crystal most of the surface is covered with reflective coating, so the beams were focused in the transparent part in the left

3.2 Spectral Hole Burning

In order to investigate phase conjugation due to off-resonant interactions (Slow-light experiments, Sec. 4.5 and 5.6), *spectral hole burning* was used to remove the ions and tailor the absorption profile near the resonant frequency. Unwanted hole burning was also observed almost in all experiments performed, so it is important to briefly discuss features of this process.

When rare-earth (RE) ions are doped into a host material their absorption line becomes *inhomogeneously* broadened (Figure 3.3). This is due to the fact that the crystal lattice is not perfect and different ions will have different surroundings and

thereby experience different static electric fields. They will then be Stark-shifted and thus have different energy levels and resonant frequencies.

Figure 3.3: Inhomogeneous broadening of absorption profile with a spectral pit (not drawn to scale). Figure adopted from [39]

When an optical field of linewidth $\Delta\nu$ propagates through the crystal, it removes absorbers from the ground state within a $\Delta\nu$ wide spectral region in the absorption profile, i.e., creates a *spectral hole*. For subsequent optical fields, this region will be transparent as long as absorbers are absent in the ground state of the transition. As was briefly mentioned before, such large change in absorption at the hole edges will also influence the real part of electric susceptibility and thus the effective refractive index through Kramers-Krönig relations [13] and the light will be slowed down.

The inhomogeneously broadened linewidth can be viewed as a sum of homogeneous broadenings from each dopant ion. An important property of RE ions is that they have long coherence times and thus relatively narrow homogeneous linewidth at liquid helium temperatures. This allows to address and selectively excite different groups of ions (and thus burn spectral holes and pits of the desired width in different parts of the inhomogeneous profile) by tuning the frequency of incoming optical field [39].

3.3 Laser system and optical setup

The laser system in use is a Coherent 699 ring cavity dye laser. It is tuned to Pr^{3+} ion resonance frequency ($\lambda = 605.97$ nm) and uses Rhodamine 6G dye as a gain medium. The average laser output power is 350 mW. The laser is stabilized in frequency by locking to a stable external cavity (Pound-Drever-Hall technique which generates sidebands to the carrier laser frequency, looks at the change in reflected power and gives proper feedback which helps to suppress frequency fluctuations) [40]. Laser locking improves the stability of the phase-conjugated signal dramatically. The optical setup layout is illustrated on Figure 3.4.

The beam from the laser is guided by the fiber to the experimental table and is split by a 10/90 beam splitter (BS) with the majority of the power transmitted to pumps and the rest is reflected to probe. The transmitted beam is then divided into forward and backward pumps by a 50/50 BS. The three beams were focused on the crystal through the cryostat windows with a pair of lenses with $f = 50$ cm. To be able to change the beam intensities, variable attenuators (rotating wheels with

transmission gradient) were used to vary the intensity of each beam. The phase conjugated signal is picked off by a BS placed in the path of the probe beam and is guided to the detector (13). The detector (10) serves as a reference detector for the probe. Detector (17) measures transmitted probe beam and is needed to observe and adjust spectral pit creation process in slow light experiments as well as to compare transmission signal with and without phase conjugation. Incoming probe intensity was measured on the PC detector with the usage of the flipping mirror (22). In the 6-mm crystal intensity measurements, forward and backward pump references were also obtained by using beam samplers and guiding the reflected part to separate detectors. In polarization experiments, three Half-Wave retarders were implemented to rotate the polarization of each beam.

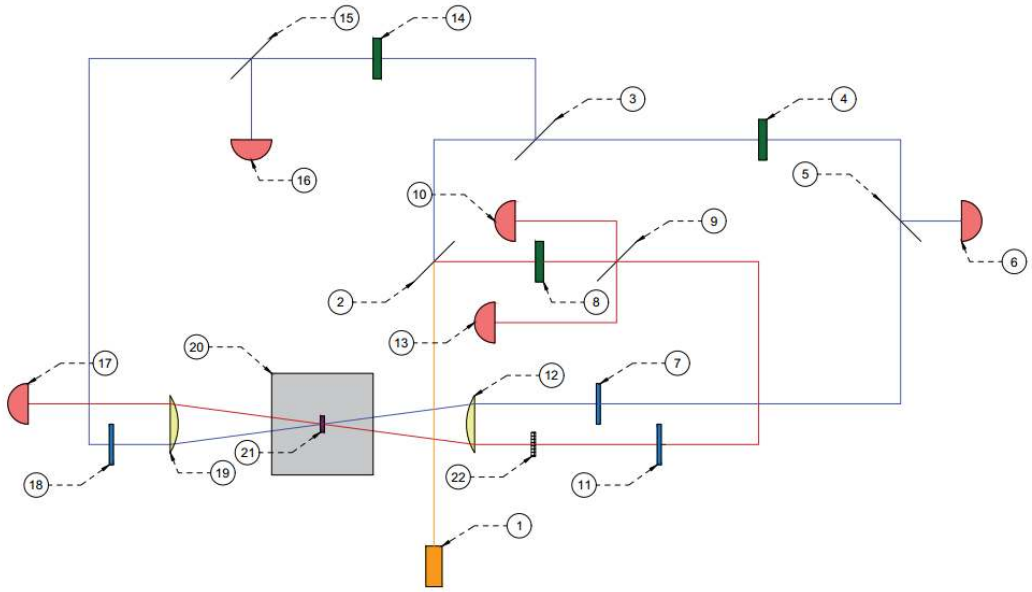

Figure 3.4: Experimental setup. Red lines denote the path of the probe, blue - the pumps. 1 - optical source, 2 - 10/90 BS, 3,9 - 50/50 BS, 4,8,14 - attenuator wheels, 5,15 - beam samplers, 6,10,16 - reference detectors, 7,11,18 - half-wave plates, - probe reference detector, 12,19 - 500 mm plano-convex lenses, 13 - PC signal detector, 17 - probe transmission detector, 20 - cryostat, 21 - crystal, 22 - flip mirror

Experiments were done in pulsed mode with a pulse duration ranging from 1 - 50 µs with a square temporal profile. Pulse control and shaping is achieved by two acousto-optical modulators (AOMs) controlled by an Arbitrary Waveform Generator (AWG), which is programmed externally by means of MATLAB™. Detectors were connected to a Teledyne LeCroy oscilloscope to collect the signal and save corresponding measurements.

3.4 Beam overlap

In order for the beams to interact with each other, they should all overlap spatially inside of the non-linear medium. The following calculation estimates the spatial overlap distance (L on Figure 3.5) and the overlap area of the interacting beams. This very simple but useful calculation allows one to get an idea about preferable

sample dimensions and thickness as well as average intensity for each beam in the crystal.

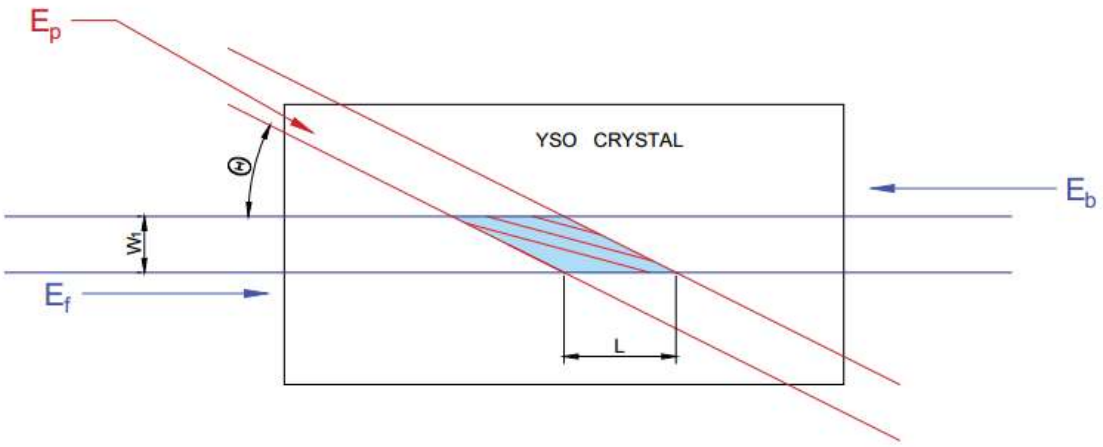

Figure 3.5: Schematic of spatial overlap between E_p, the probe wave, and E_f, E_b - forward and backward pumps, Θ - angle between E_p and E_f, L - overlap distance along direction of propagation, W_1 - diameter of the beams after the focusing

We start with obtaining data for incoming laser beams: the average power of the collimated beam after the fiber is in the range of 10-12 mW, after splitting (before the cryostat) - approximately 3-3.5 mW for the pumps and 0.7-0.9 mW for the probe. The beam diameter for each beam was approximately 2.8 - 3 mm; the spatial intensity profile is roughly Gaussian TEM_{00} mode. Previous to the experiments, spatial intensity profiles of the beams were recorded with a laser beam profiler camera (Figure 3.6).

To calculate Θ, F and P beam separation was measured and turned out to be equal to 17 mm before the lens ((12) in Figure 3.4). This gives $\Theta = 1.94°$ for the 500-mm lens. Taking into account the Gaussian profile, formula for estimating beam radius in the lens' focal point:

$$W_1 = \frac{\lambda f}{\pi W_0} \tag{3.1}$$

Where, $\lambda = 606$ nm, $f = 500$ mm, $2W_0 = 3.06$ mm. Thus, $2W_1 = 128$ µm. By means of simple geometry it is not hard to estimate L = 3.82 mm and area A = 0.48 mm^2.

In theory, it means that for the 6-mm-thick crystal the beam overlap length is less than the crystal thickness. This may cause some unwanted absorption in the conjugate signal. For the 1-mm-thick sample, the beams cover all of its thickness and there is more translational freedom in the focusing lens position along the direction of propagation.

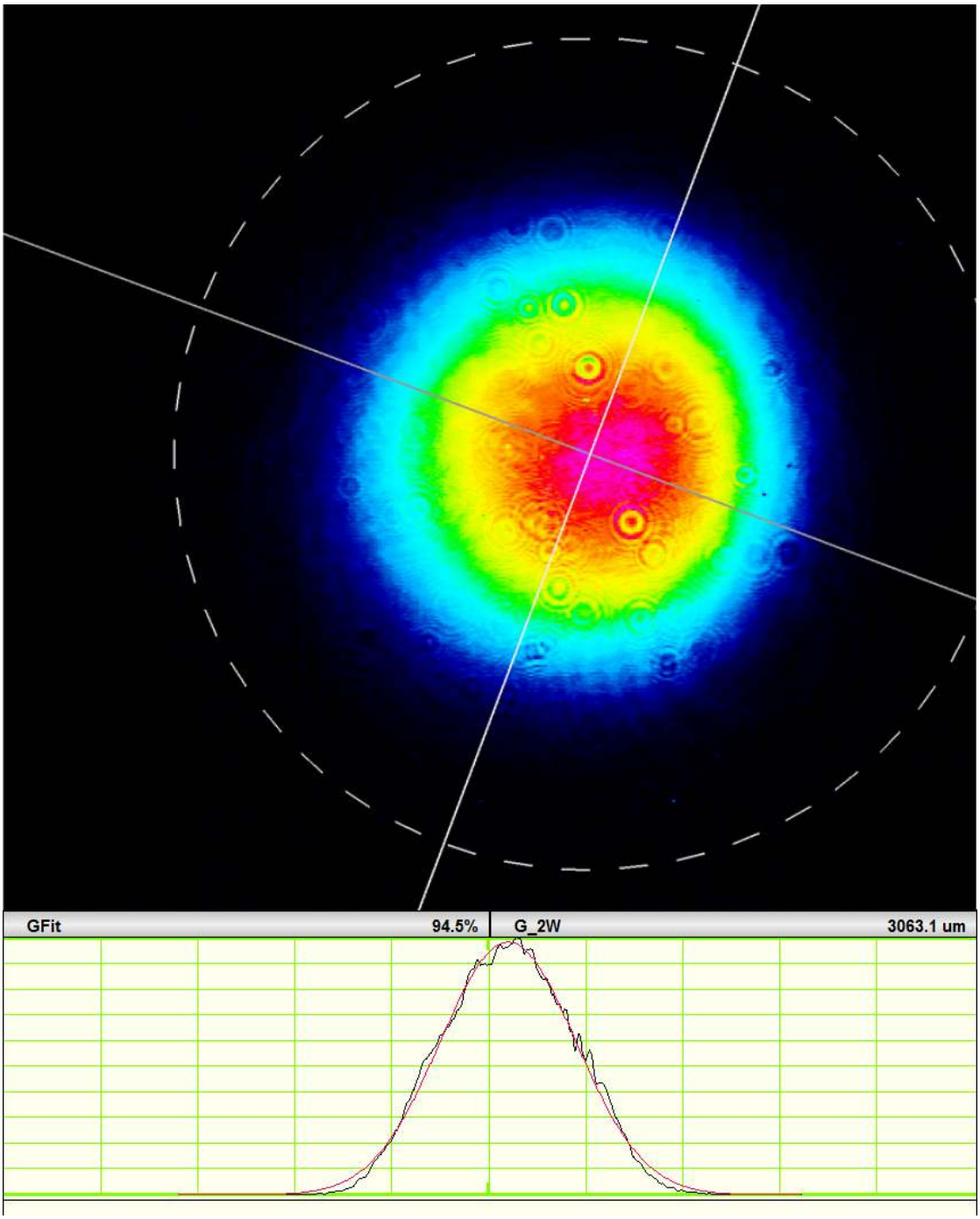

Figure 3.6: Spatial intensity profile of incoming beams. Data average of 20 shots. Top - image of the intensity profile, bottom intensity profile with Gaussian Fit. GFit - fit of the data to the Gaussian curve(in %), G_2W - beam diameter

Chapter 4

Results and discussion (1 mm crystal)

4.1 Signal structure. Efficiency

In the first experimental session, a crystal with a thickness of 1 mm was studied. After optimizing the optics to remove unwanted background light, the phase-conjugated signal structure was recorded and is shown in Figure 4.1.

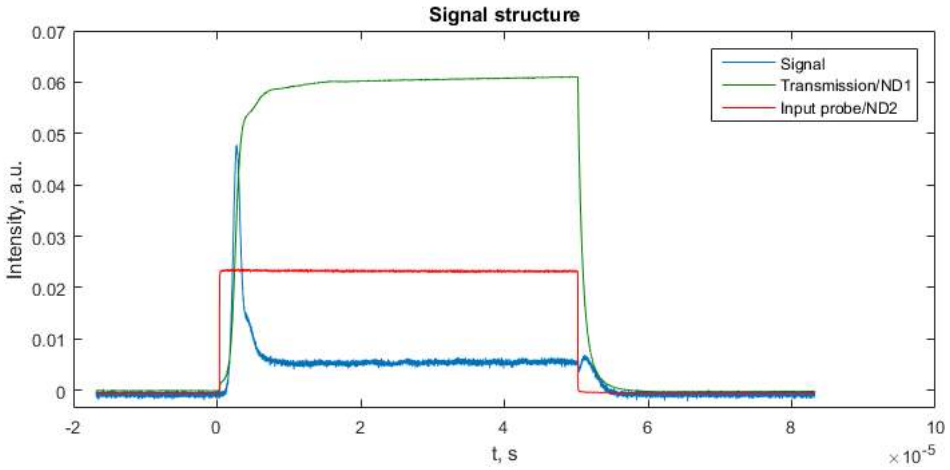

Figure 4.1: Phase conjugation in the 1-mm-thick crystal. Pulse duration - 50 μs, transmitted probe is attenuated 10 times, incoming probe - 100.

Overall, this signal has a few distinctive features - a strong peak at the beginning of the pulse, a weak steady-state signal, and a small peak at the end, right after the excitation pulses are turned off (compare the signal to an input probe reference pulse). Note that the probe transmission curve experiences a small dip at the beginning which correlates with the phase-conjugated peak time-wise.

As was mentioned before, in this crystal the D2 axis coincided with polarization of each beam. It was later established that efficiency-wise, it is the least effective setup (Section 5.5) but at the same time it carries the fastest response (compared to that of a 6-mm-thick sample) - the signal reaches its peak value approximately after 1.5 μs. This transient response could be explained as a buildup followed by saturation and depletion of the population grating. As the pulse starts, it takes

a short time to create an effective population grating structure since the beams propagate along the highly absorptive principle axis, however shortly after, this structure is destroyed by those excitation pulses.

The second peak is rather difficult to explain. It appears that it is a signal from a photon echo type process emitted in the opposite direction of the probe beam. In other words, phase information of the three excitation pulses is stored in the excited Pr ions which later re-radiate coherently to produce another phase-conjugated pulse similar to the one we see in the beginning. One possible suggestion to study the properties of this second peak is to slightly shift the central frequency of an incoming laser field within the MHz range using the AOMs. This measurement can tell how strongly that second peak intensity depends on the detuning from the ion resonance. A similar experiment is described below, but for this sample there were only 3 data points taken with frequency steps of a couple GHz by locking to the different cavity modes of the laser system.

Reflectivity (efficiency) of the phase-conjugated signal was calculated as the ratio between the signal intensity and the incoming probe. Compensating for the losses on cryostat windows (approximately 50% of the input intensity for a double pass), the reflectivity was roughly equal to 4.1 % which is comparable to the previous results obtained in the group a few years ago (4.5 - 5 %).

4.2 Absorption

One of the ways to characterize the resonant nature of the DFWM process in these crystals is to measure the signal intensity as a function of absorption which can be mimicked by shifting the laser central frequency away from the Pr ion resonance. Figure 4.2 shows the signal structure for three different frequencies of an incoming laser light with normalized peak intensity shown on the subplot.

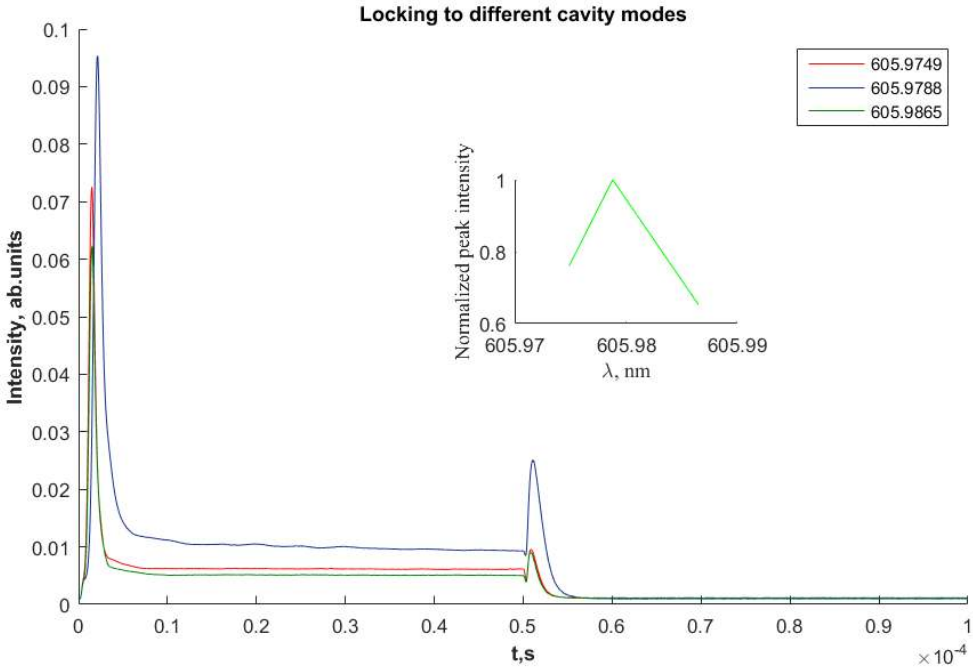

Figure 4.2: Signal structure as function of incoming laser frequency

Praseodymium ions have atomic resonance roughly at 605.9787 nm, and, as can be seen from the plot, the intensity around this point is the highest. Going either higher or lower in frequency from the resonance decreased the signal by a significant margin, so further experiments were performed with the laser locked close to resonance. One feature that can be noticed is that the difference between the second peak intensity on and off resonance is bigger compared to that of the first peak. The obvious improvement to this experiment is to obtain more data points (probe Pr inhomogeneous absorption profile more accurately) and study phase conjugation further away from the resonant frequency and also at intermediate positions in the inhomogeneous absorption profile. However, in author‘s opinion there will be no qualitative or quantitative improvements to the signal when going away from the resonant transition.

4.3 Pulse Duration

One of the simpler experiments that can be done is to vary the temporal width of the incoming laser pulses. The signal intensity as a function of the pulse duration is shown in Figure 4.3. In this measurement, pulses of a narrow spectral width (largely Fourier-limited) were used.

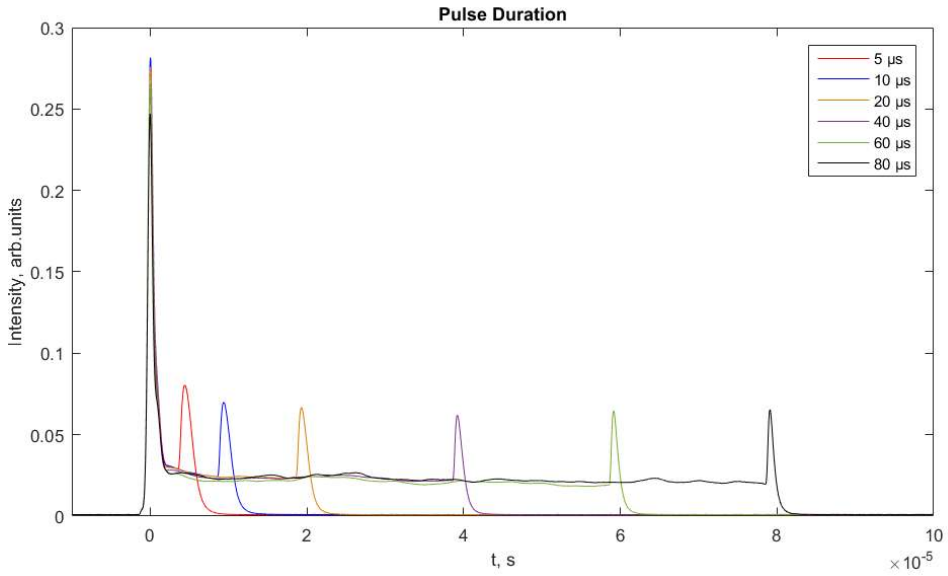

Figure 4.3: Signal structure with pulses of different width.

As can be seen, the signal does not change qualitatively and keeps the same structure as the pulse width increases. As the response from this crystal is rather fast, it would be of immense interest to try 1-2 μs or even shorter pulses and look at the resulting signal structure (this was partly done for the 6-mm-thick sample). During the experiments on a 6-mm crystal (Section 5.2) it was established that chirping the laser frequency significantly affects the phase-conjugated signal structure. Thus, it would be rather useful to do the same measurement for the 1-mm-thick sample as well - it was partly done earlier in the group but without locking the laser.

4.4 Rabi frequency. Incoming beam intensity

In the following section, the phase-conjugated signal was studied as a function of an incoming Rabi frequency and beam intensity. The Rabi frequency is proportional to an amplitude of an electric field and describes the strength of coupling between an atomic transition and a perturbing field [41]. Simply put, decreasing (increasing) the Rabi frequency will decrease (increase) the amplitude and thus the intensity of all three incoming beams. In Figure 4.4 below, the signal grows monotonously with increasing Rabi frequency, as expected. From theory described in Section 2.1, signal intensity should grow as a 6th power in respect to the increase in Ω_{Rabi}, although it is not observable on this plot. This indicates that the case of the resonant DFWM cannot be described with the simple approach given in Section 2.1. In principle, in this instance, it would be incredibly helpful to do an analytical or numerical calculation and compare the results with obtained experimental data.

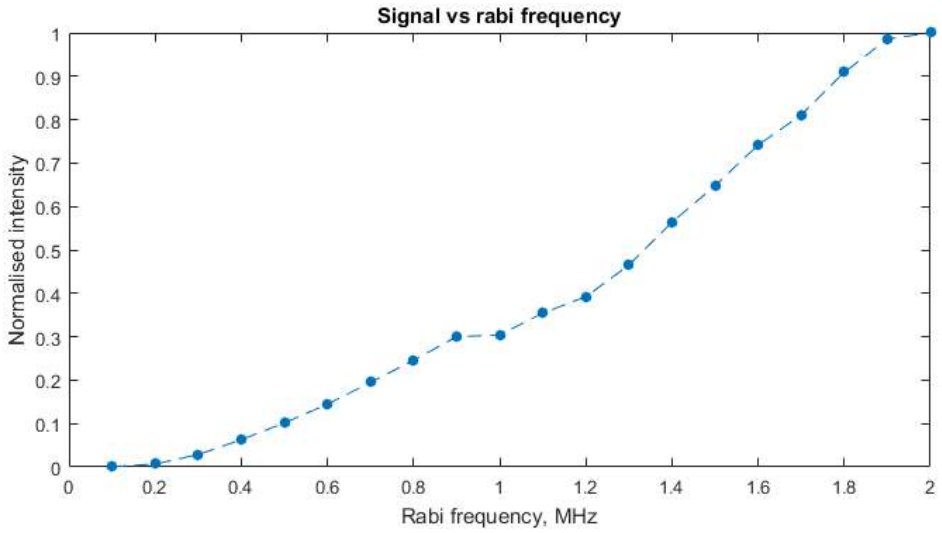

Figure 4.4: Signal intensity as a function of Rabi frequency

Dividing the signal by the probe reference intensity, it is possible to obtain an efficiency curve (Figure 4.5):

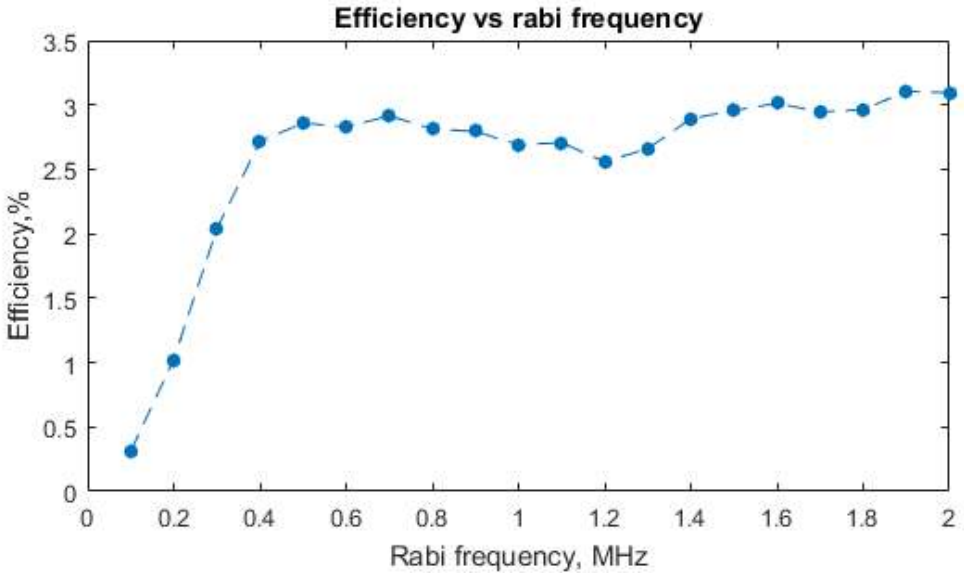

Figure 4.5: Phase conjugation efficiency as a function of Rabi frequency

It is clear that the phase conjugation is much less efficient in the low-intensity optical field regime, with efficiency dropping almost an order of magnitude. This could be explained by considering the fact that if the Rabi frequency of the incoming electric field is too small, it would not be able to successfully excite a sufficient amount of ions and thus create an efficient population grating. As Ω_{Rabi} increases, efficiency "saturates" and only fluctuates slightly.

The next step was to change the intensity of the beams separately. In the 1-mm crystal, this was done for the probe and the both pumps. In accordance with the theory (Section 2.1 and 2.2), varying intensity of one of the input beams would induce a linear change in the signal until the medium gets saturated. Experimental results for the probe beam intensity sweep show that it is indeed the case. In the

Figure below, the phase-conjugated signal is plotted as a function of the reference probe beam intensity.

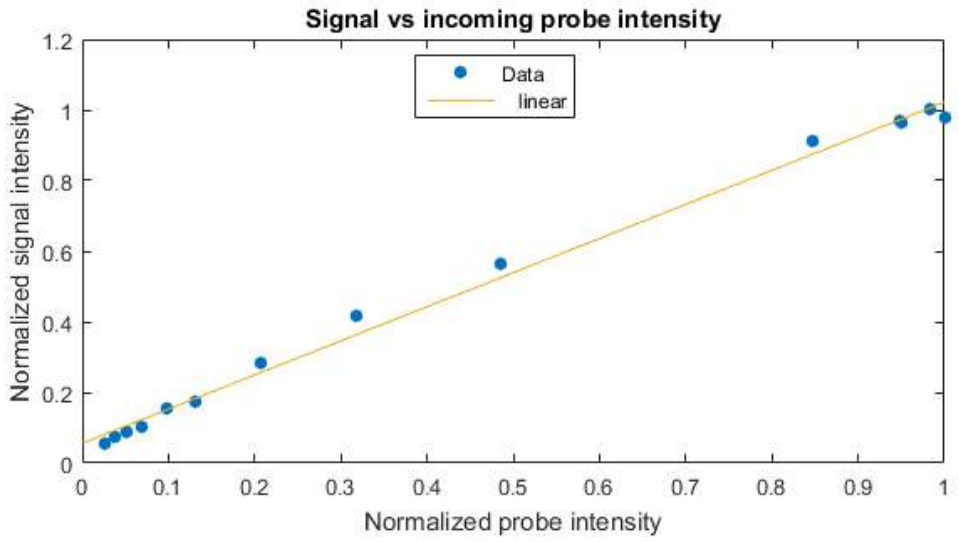

Figure 4.6: Signal as a function of incoming probe intensity

As can be seen from the plot, the probe beam does not saturate the signal as it (the probe) is rather weak (approximately 10-15% of initial power after the fiber) compared to the pumps.

For the 1-mm-thick sample, pump beam intensities were altered simultaneously by placing the attenuator wheel before BS (3) in Figure 3.4 (opposed to separate measurements for each of the pumps in 6-mm crystal experiments).

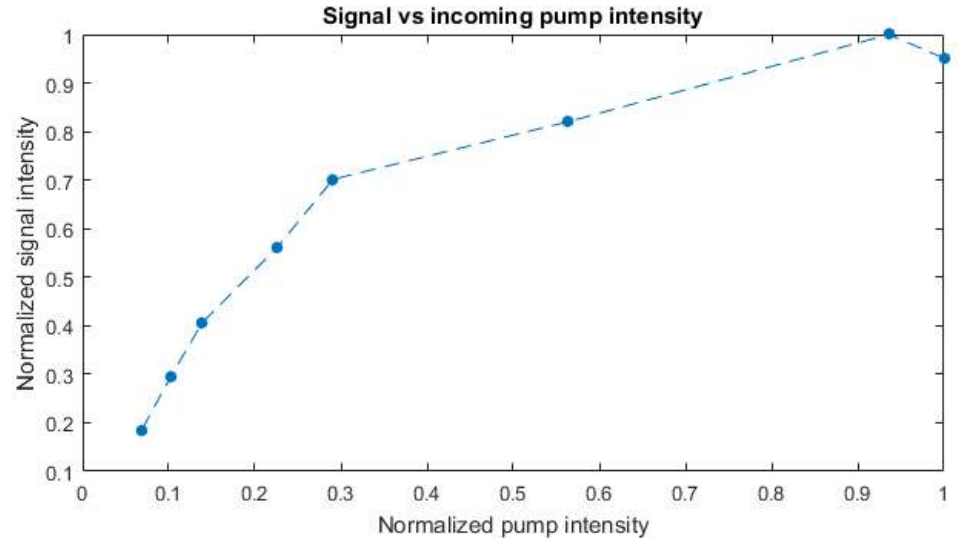

Figure 4.7: Signal as a function of incoming pump (both B and F) intensity

Figure 4.7 shows that in the range of low pump intensities the signal grows more or less steadily and although it seems to look linear, one should be careful with the assumption of a linear trend here as both the pumps were changed simultaneously, so in theory the expected dependence is quadratic. As the pump intensity value reaches its available maximum, the signal stops its growth, i.e.

saturates. The obvious improvement to this measurement is to vary and measure the beam intensities of the pumps separately - this, in turn, will provide more insight on the individual contribution of each beam to the signal.

4.5 Slow light experiments

In the succeeding section, the phase-conjugated signal properties due to non-resonant interactions are discussed. In order to study these properties, spectral pits of different widths were burnt in the inhomogeneous absorption profile of the crystal. One example of such a pit is presented in Figure 4.8. Inside the pit, a group velocity of propagating light pulse is proportional to the pit width, $v_g \propto \Gamma$, so by changing the spectral width of the pit it is possible to vary the propagation velocity of the phase-conjugated signal.

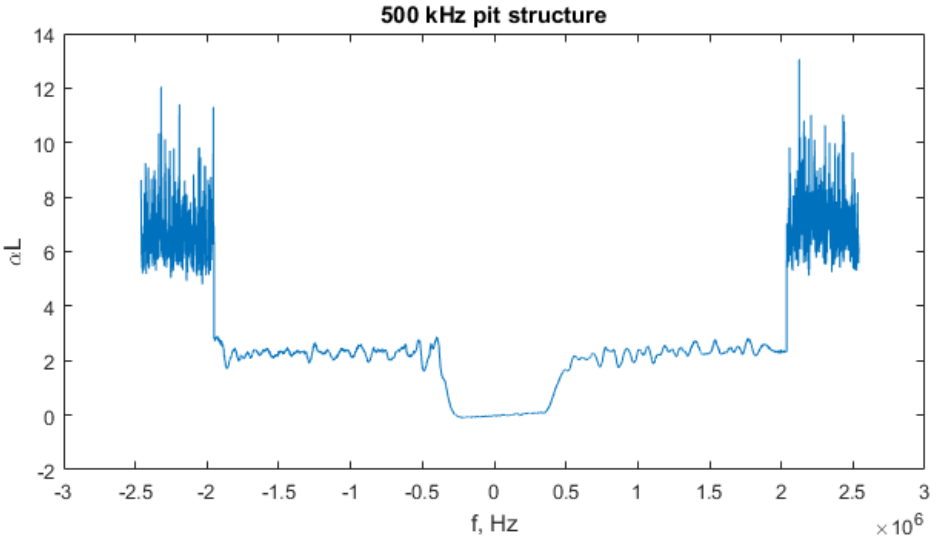

Figure 4.8: 500 kHz pit structure

In the following experiment, the 500 kHz-wide pit was burned and the phase-conjugated pulse was sent into different parts of the pit (the pulse center frequency was shifted with 100 kHz steps across the pit). Notice that the pit structure is not completely flat, but contains a small slope, with absorption values being slightly higher on the right side of the pit. This slope is possibly the reason for a difference in intensity for symmetric values of the frequency shift (e.g., the signal from -0.1 and 0.1 MHz shifts should, in theory, be the same, but in reality the signal with the 0.1 MHz detuning is slightly stronger), shown in Figure 4.9

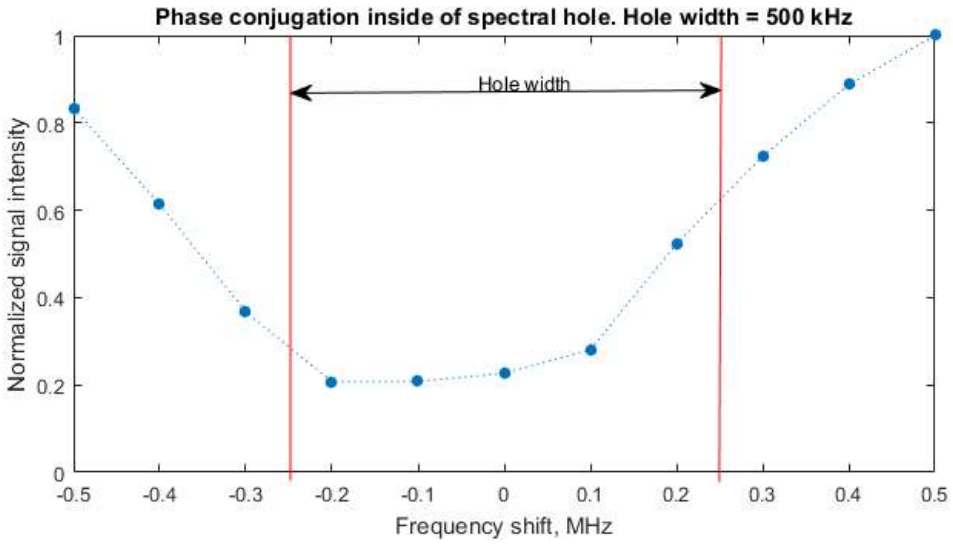

Figure 4.9: Phase conjugated signal intensity as a function of frequency shift inside of 500 kHz spectral pit. Pit borders are marked with vertical red lines

It is evident from the plot above that the signal is the lowest when its center frequency coincides with the pit's center. As in the absorption experiment discussed earlier, it also proves the strong resonant nature of DFWM process in Pr^{3+}:Y_2SiO_5. It also supports the "phase conjugation by population grating" picture: by burning a pit, we remove the ions needed for the grating creation to other hyperfine levels making them unavailable to incoming optical fields. Closer to the pit's edges the signal is stronger compared to that in the center because the burning process is not ideal - there are more ions in the ground state remaining there. This could also be the reason why there is still some signal in the middle of the pit, although here the steady-state was almost as dominant as the first resonant peak in Figure 4.1.

Figure 4.10 shows the signal intensities while propagating in the pits of 1,2 and 4 MHz width.

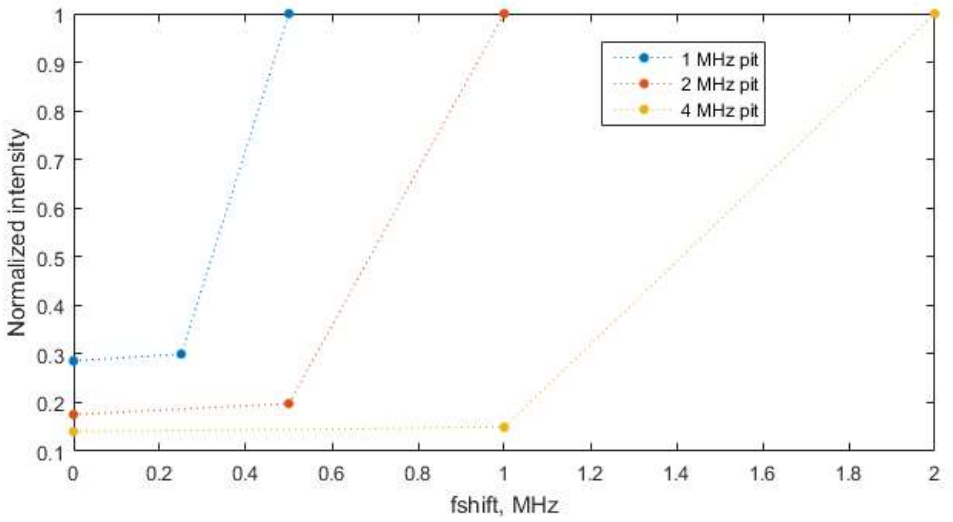

Figure 4.10: Signal intensity as a function of frequency shift in pits of different width. $fshift = 0$ - center of the pit.

In every case, the signal in the pit‘s center and in the area between the middle point and the edge is significantly weaker compared to the edge signal intensity. It can be argued that the signal is the weakest for 4 MHz pit because the burning process is the more efficient for the wider pits than for the narrower ones (more ions were removed from the resonant transition).

Chapter 5

Results and discussion (6 mm crystal)

5.1 Signal structure

For the 6-mm-thick crystal first experiments were carried out with the S polarized beams (in respect to the plane of the optical table) so that the incoming light is polarized neither along the D1 nor the D2 principal axis, although by looking at Figure 3.1 it is clear that the incident polarization is closer to the D1 axis. It was determined that the light polarization severely affects both the signal structure and its strength; therefore, the signal efficiency was studied later (Section 5.5).

The phase-conjugated signal structure for the 6-mm-thick crystal is shown in Figure 5.1. The obvious difference from the signal curve obtained in the 1-mm sample is a substantially stronger steady-state signal (approximately 50% of the peak signal intensity) and a slower response to the excitation pulses: the first peak comes roughly 6 µs after the reference pulse triggers the oscilloscope (compare the delay between the peak and the reference). The first feature could be explained by considering the fact that now the light polarization is aligned closer to the D1 axis which is the least absorbing principal axis. Hence, this steady-state signal is absorbed much less by the crystal. A time delay, in theory, can be connected with propagation in the slow-light regime, discussed further in Section 5.3.

After the excitation pulses end, there is still some light coming out of the crystal which can be seen both on the signal and transmission curves. Note that due to the stronger steady-state, there is a clearly observable exponential decay in the signal and transmission which can be explained by coherent radiation from excited the Pr ions (free induction decay). After this decay, there is a small bump in the signal curve which is possibly of the same nature as the second peak from the 1-mm sample measurements described in the previous chapter.

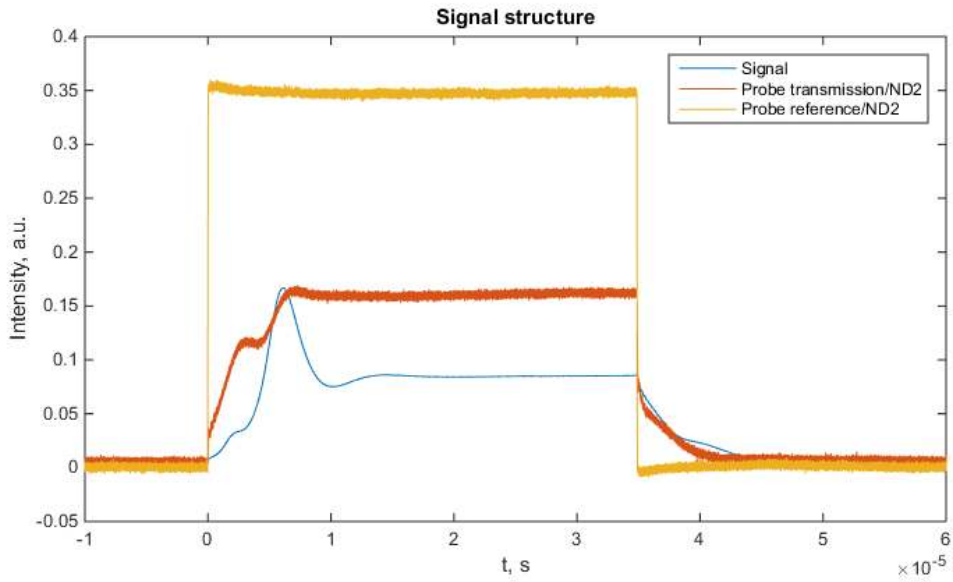

Figure 5.1: Signal structure for 6-mm-thick sample. All beams are S polarized. 35 µs pulse duration. Transmission and reference signals are attenuated 100 times.

5.2 Chirp rate

As was briefly mentioned in Chapter 4, chirping the pulse, i.e. changing its instantaneous frequency in time, qualitatively affects the structure of the phase-conjugated signal, as shown in Figure 5.2.

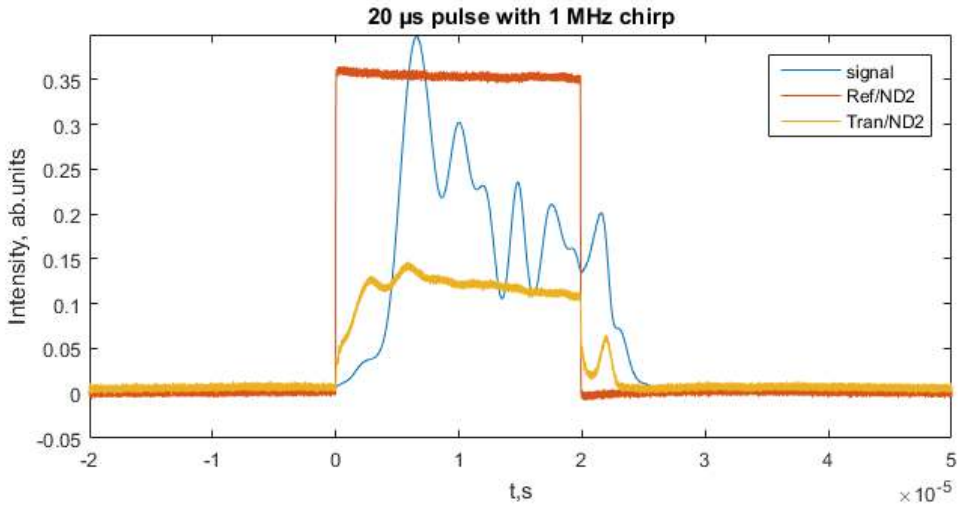

Figure 5.2: Signal structure of incoming 1 MHz-chirped pulse

Now the signal has a series of peaks instead of just one as in the unchirped case. This is due to the fact that when the frequency of the pulse is changed, this pulse starts to excite different groups of ions with different resonant frequencies. Note that there is also a peak in the probe transmission which correlates with the last peak of the conjugated signal. It is not entirely clear what could be the reason for this behaviour, but one hypothesis is that when the conjugated signal is created inside of the crystal, it also creates a grating with the pumps similar to the one

described earlier. This grating will scatter one or partly both of the pumps into a phase-conjugate version of the signal which is the probe.

While chirping the pulse can in theory be beneficial for increasing efficiency or getting the signal structure of the desired shape, one should be careful not to chirp the pulse too rapidly. For the previously used 20 µs pulse, Figure 5.3 shows the effects of changing the chirp values in the range of 1-10 MHz.

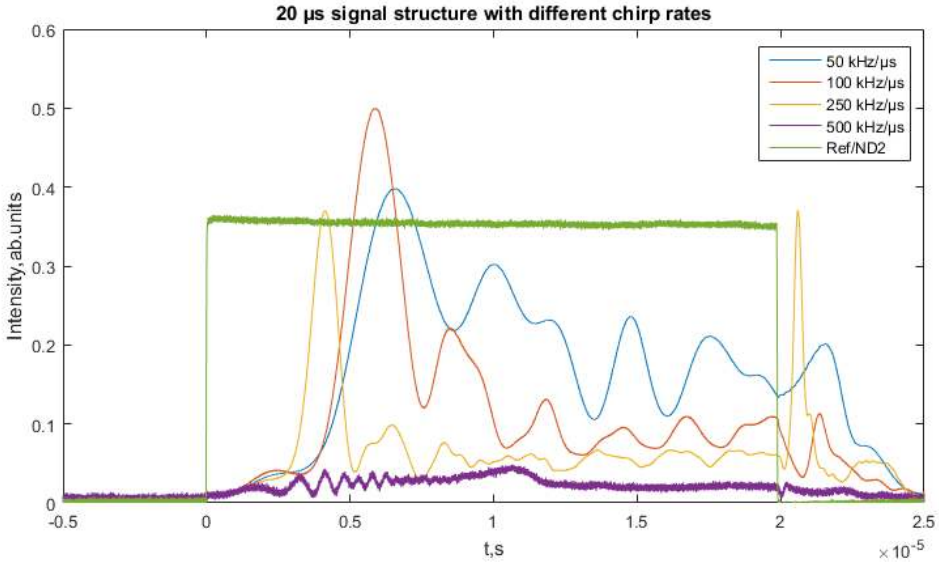

Figure 5.3: Signal structure for different chirp values

The 10 MHz signal in the figure above is almost negligible compared to the other curves. Indeed, when one changes the instantaneous frequency too fast (500 kHz/µs in this case), the pulse simply doesn't have enough time to interact with one group of ions before switching to the other one. The strong second peak in the 5 MHz-chirped pulse is surprising and rather difficult to interpret. In order to understand it better, further studies of this particular signal should be carried out, e.g. changing the polarization or the Rabi frequency of incoming beams or shifting the center frequency of this pulse.

When comparing the chirped signal structure with the unchirped case, it becomes clear that in this scenario, chirping the pulse not only changes its shape but also gives a boost to signal strength. The peak from the 2 MHz-chirped signal is almost 3 times stronger than the unchirped one, and a 2 MHz chirp seems to be a near optimal value for this pulse duration which gives the chirp rate of 100 kHz per µs. In order to investigate which chirp values give the highest efficiency, more precise measurements have been taken, and the results are shown in Figure 5.4. Note that in this case, the pulse duration was 15 µs so this plot should not be compared to the results presented above (where e.g. the 2 MHz-chirped pulse is clearly stronger than the 1 MHz one).

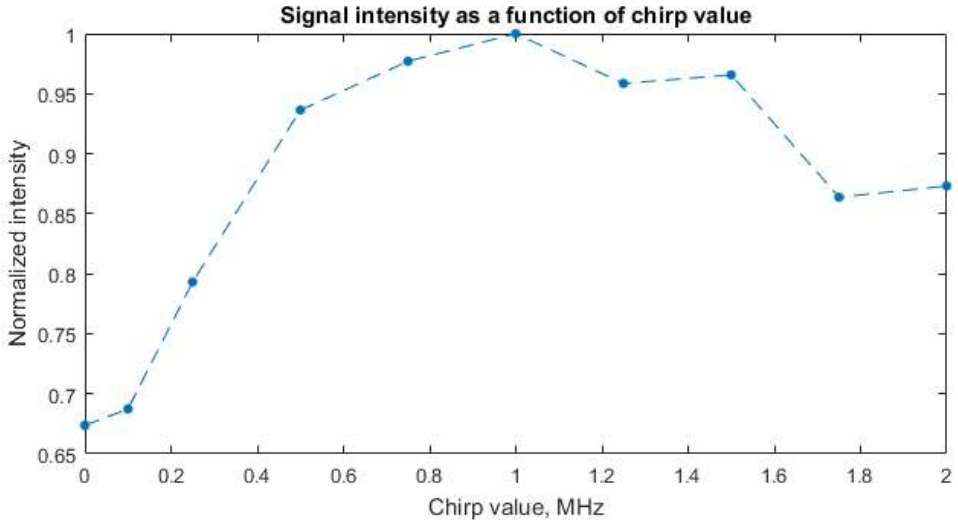

Figure 5.4: Signal intensity as a function of chirp value for 15 µs *long pulse*

The maximum peak intensity for the 15 µs long pulse was obtained with the 1 - 1.5 MHz chirp values. This gives the optimal chirp rate value approximately equal to 70 - 100 kHz/µs which agrees with the observation for Figure 5.3. Increasing the chirp rate in Figure 5.4 led to a decrease in signal intensity which means that the faster chirp rates are not as efficient, as was explained before.

5.3 Pulse duration

Compared to the 1-mm-thick crystal (Section 4.3), in this session, the phase-conjugated signal was studied as a function of the pulse duration with both chirped and unchirped cases. Figure 5.5 illustrates the signal from unchirped pulses of a 5-50 µs temporal width. As was mentioned before, the steady-state signal is significant here, and the difference in the peak‘s height for different pulse widths is more pronounced than that of a 1-mm sample. Due to a rather slow response, 5 and 10 µs long pulses do not possess a steady-state signal present in the other pulses. Otherwise, the qualitative picture does not change, which is comparable to the results for the thin crystal.

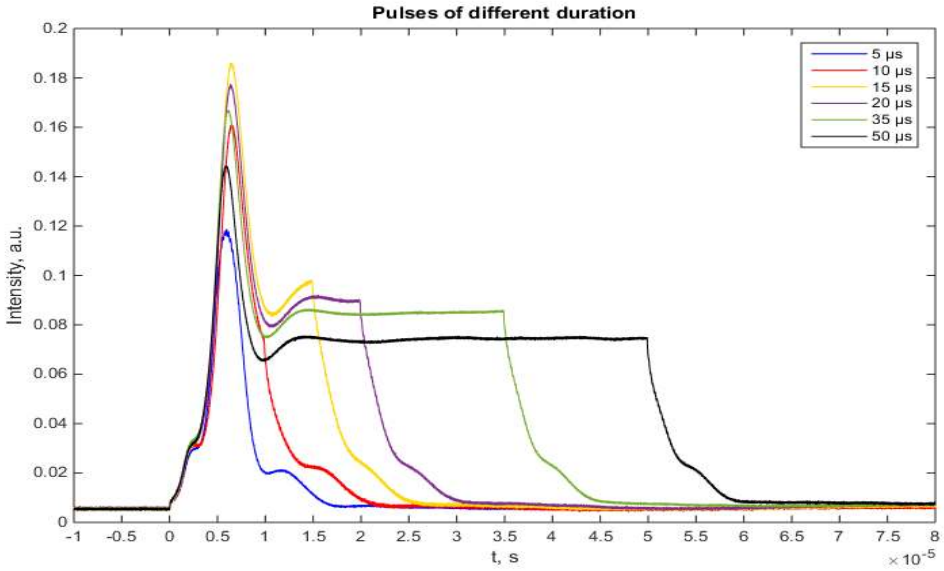

Figure 5.5: Signal structure as a function of pulse duration (unchirped)

By looking at the time scale in Figure 5.5 one can notice a substantial delay between the phase-conjugated signal and the reference pulse. Figure 5.6 shows a signal from a 5 µs long incoming pulse compared to its reference.

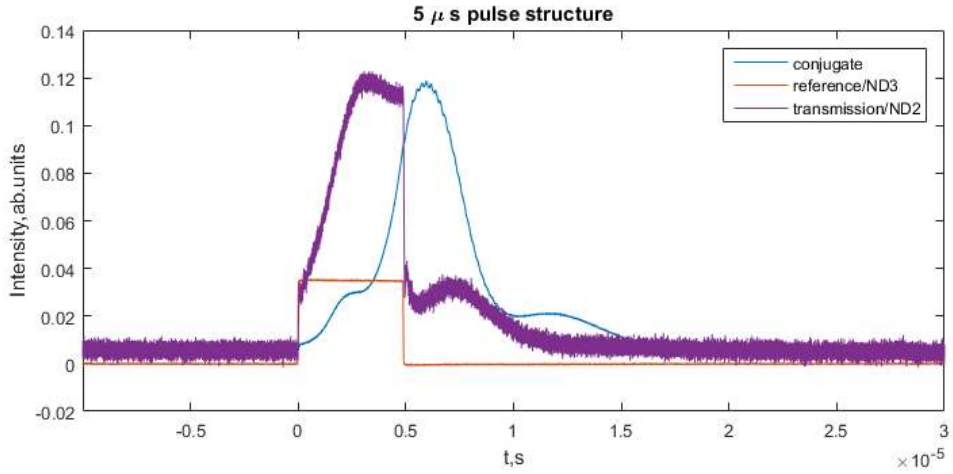

Figure 5.6: Signal structure of 5 µs long pulse. Transmission appears noisy due to not being averaged

It is evident that the signal peak comes after the reference pulse ended completely. In theory, it can be connected to two things that were briefly mentioned earlier. The first guess would be that on the way out of the crystal the conjugated wave is travelling in the transmission window burned by the probe beam, so its group velocity is reduced significantly. The second reason might be connected to the light polarization - the D1 axis is highly transmissible so it will take a longer time for the pulses to create an effective population grating in the overlap region. It is not completely obvious what is the actual reason for this time delay, in principle it can be both of these effects contributing equally or one effect could be dominated by the other one. To understand this deeper, further experiments

have to be carried out. One could try to get a measurement of the time delay as a function of the laser beam angles - changing the angle between the forward pump and the probe will shift the overlap region's position and thus the distance that a conjugate wave has to cover inside the crystal. The other thing to check would be the time delay as a function of the beam intensities e.g. changing the probe beam intensity could influence an effectiveness of the hole burning process in the crystal and thus will affect the light velocity of the conjugated wave travelling inside of this spectral hole.

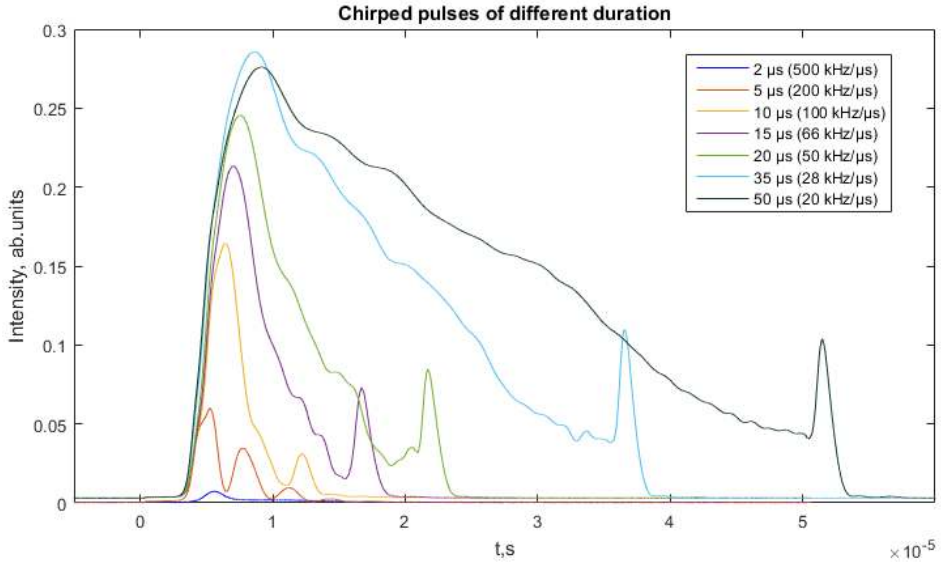

Figure 5.7: Signal structure as a function of pulse duration (1 MHz chirp). BWP along D1 axis

Figure 5.7 shows the phase-conjugated signal for 1-MHz-chirped pulses of a 2-50 µs temporal width. The secondary peaks within the pulses are much less definitive because in this experiment the backward pump beam polarization was turned to coincide with the D1 axis of the crystal which enabled a strong steady-state signal (See Section 5.5). It is not hard to notice that for the short (2-15 µs) pulses, the signal structure differs significantly with increasing duration; for longer pulses, the signal structure looks more or less the same. Also, here the signal strength varies greatly when changing the pulse duration but this was expected - the chirp value for this measurement was kept constant and, as discussed before, the optimal chirp rate is different for pulses of different duration. Thus, a general enhancement of this measurement would be to tune the chirp rate to fit the pulse duration accordingly.

5.4 Rabi frequency. Beam Intensity

As was discussed in the respective section for the 1-mm-thick sample, varying Rabi frequency essentially changes the intensities of all incoming beams. Figure 5.8 shows the signal intensity as a function of incoming Rabi frequency.

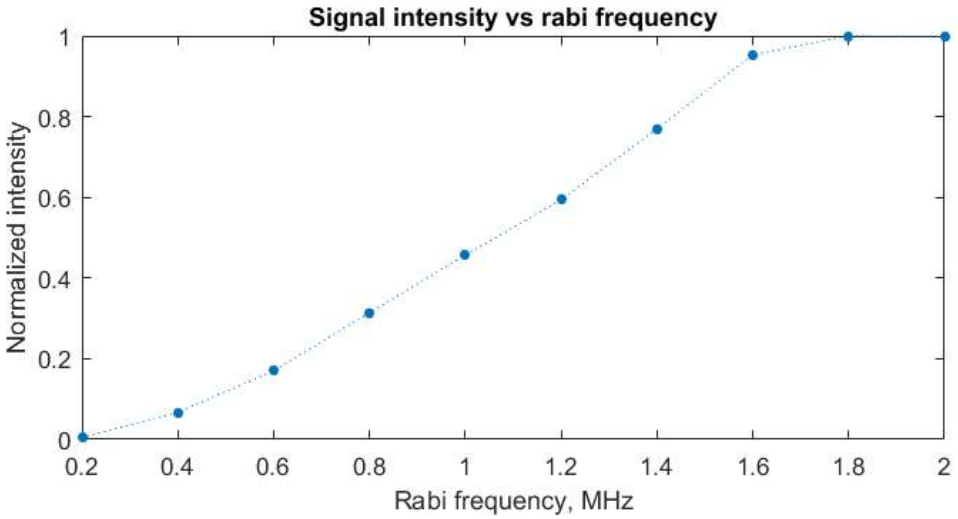

Figure 5.8: Normalized signal intensity as a function of incoming Rabi frequency

In general, this trend is similar to the one presented in Figure 4.4 for the thin crystal, although here the signal saturation is more obvious with the intensity reaching its maximum value in the range of Rabi frequencies of 1.6 - 2 MHz.

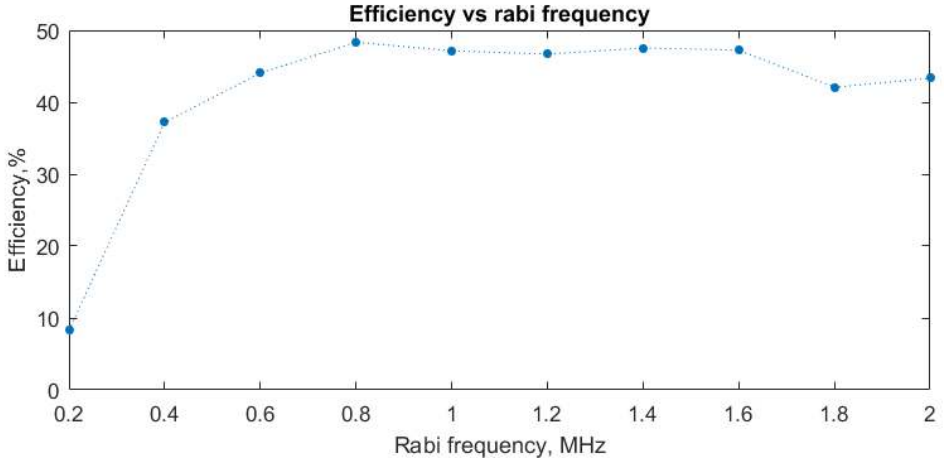

Figure 5.9: Signal efficiency as a function of incoming Rabi frequency. Here cryostat window losses were not taken into account

The efficiency curve is also comparable to the previous results with lower values in the weak-field regime (0.2-0.6 MHz) and then stabilizing afterwards. Note that in this particular experiment, all the beams were polarized along the D1 crystal axis, which later was established to be the most efficient stable signal polarization configuration (Section 5.5 for polarization studies and signal dynamics experiments) so this is mainly the reason for such high values of reflectivity (Y-axis in Figure 5.9).

The next step was to vary the intensity of each beam separately. For the probe intensity sweep, a direct comparison could be made with results from the 1-mm crystal (Figure 4.6). The normalized signal intensity as a function of incoming probe intensity is demonstrated below.

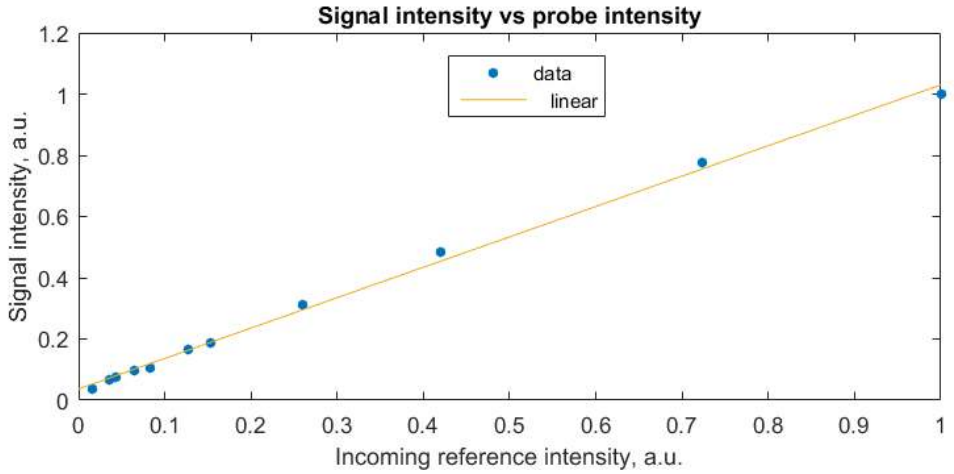

Figure 5.10: Signal intensity as a function of incoming probe intensity. Both intensity values are normalized

The linear dependence in Figure 5.10 readily agrees with both the previous measurement for the thin sample as well as the theory and no signal saturation was observed in this case either.

In order to obtain maximum efficiency of the phase-conjugated wave, it is crucial to know how the signal behaves when the intensity of the pumps is changed. Intensity dependence experiments for the pumps were done both in the unchirped and chirped regime and no significant difference was observed between the two. First, the forward pump is discussed: (Figure 5.11)

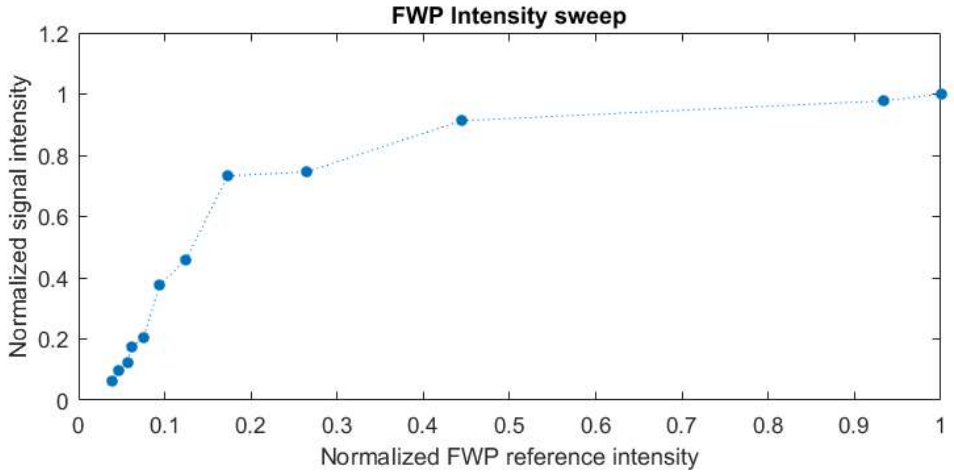

Figure 5.11: Signal as a function of incoming forward pump intensity

It is clear that the forward pump saturates the signal: when an incoming FWP intensity was lowered by a factor of 2, the signal still had almost the same value of intensity. In the weak-field regime (from 0.05 to 0.2 of the maximum intensity value) the dependence is roughly linear which is expected. In theory, it means that there is no need for increasing the power of the forward pump beam and the approximate value of 3 mW is sufficient in order to obtain an efficient signal.

Results of the backward pump intensity experiment are shown in Figure 5.12.

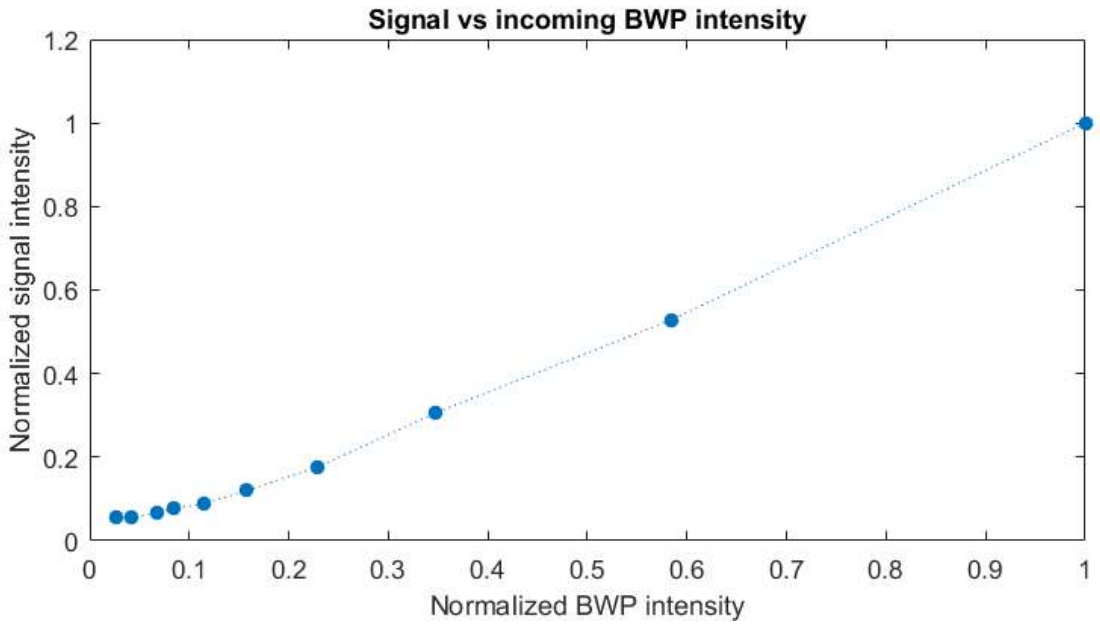

Figure 5.12: Signal as a function of incoming backward pump intensity

As can be seen from the plot, the backward pump does not saturate the phase-conjugated signal - as soon as the pump gets attenuated, the signal drops as well. This is slightly surprising considering the fact that the forward pump is saturating the conjugate and the backward pump is, in fact, the strongest beam in the experimental setup with a maximum power of approximately 3.5 mW. This leads to the assumption that the main contribution to the signal comes from the scattering of the backward pump beam from the grating created by the forward pump and the probe (the transmission grating). This assumption is also supported by polarization experiments where the change in the BWP beam induced the most dramatic changes in the phase-conjugate intensity (A further discussion is provided in Section 5.5).

5.5 Polarization. Efficiency

The polarization of incident light has a strong impact on the shape of the phase-conjugated signal and its intensity. In order to study this impact, three half-wave plates were inserted in each beam. A few quite interesting results are presented in the following section.

Figure 5.13 shows phase-conjugated signals for different polarization permutations of the incoming laser beams. The signal is the strongest when all the beams are polarized along the D1 principal axis. It was observed that this signal had the largest value of reflectivity, higher than unity - 124 % (62 % without considering losses on the cryostat windows). This could be connected with the assumption that it is still possible to create an effective population grating when propagating along the least absorbing axis and thus get the smallest reduction in the signal due to absorption. When the beams were S polarized (initial experiments), efficiency was approximately equal to 16%, which is almost an order of magnitude lower compared to the value above. It was observed that chirping the pulse with beams polarized along D1 did not give any significant boost in the signal intensity.

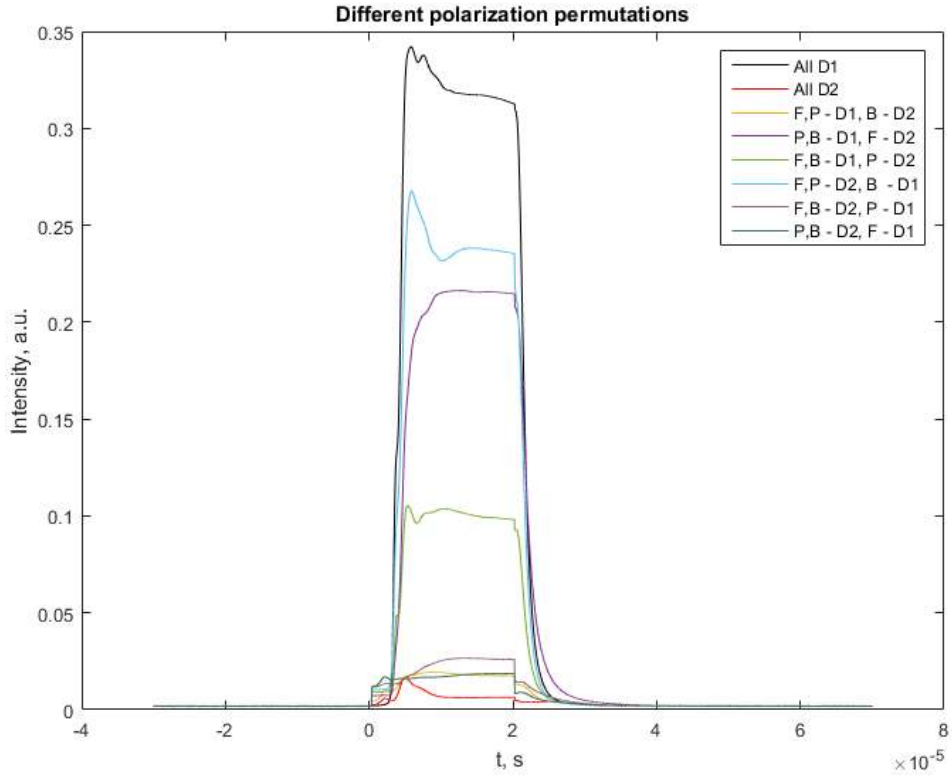

Figure 5.13: Signal structure for different polarization permutations. P is the probe, F and B denote forward and backward pump, respectively

On the contrary, the conjugate beam intensity is rather low when the polarization of F, P and B waves is parallel to the D2 axis, as was the case for the 1-mm-thick sample.

To make the analysis easier, it is useful to divide the rather busy Figure 5.13 into two separate pictures with strong-signal polarization combinations in the first plot (Figure 5.14) and the weak ones in the other (Figure 5.15). When looking at those two figures it is not difficult to notice that the obtained data has a striking feature - strong signal intensities are observed when the backward pump is polarized along the D1 axis and the signal is significantly weaker when the BWP polarization is parallel to the D2 axis of the YSO crystal. This strong impact of the backward pump polarization, in theory, can indicate that the transmission (the grating created by the F and P beams from which the B beam is Bragg-scattered into the conjugate of P) and reflection (the grating between P and B and the conjugate is obtained by the Bragg reflection of the forward pump) gratings do not contribute to the signal equally, but that the transmission grating has far a more significant impact. This loosely agrees with the experimental results obtained by Green *et al.* on Nd:YAG crystals [42] where reflectivities from transmission gratings were also observed to be higher than that of their reflective counterpart.

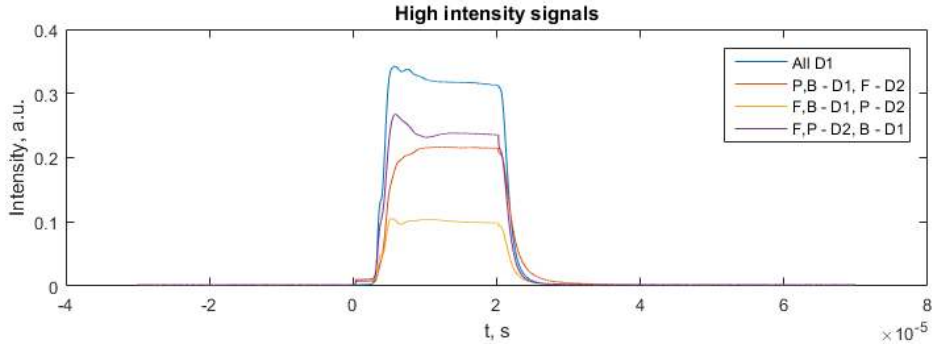

Figure 5.14: Polarization permutations that give stronger signal

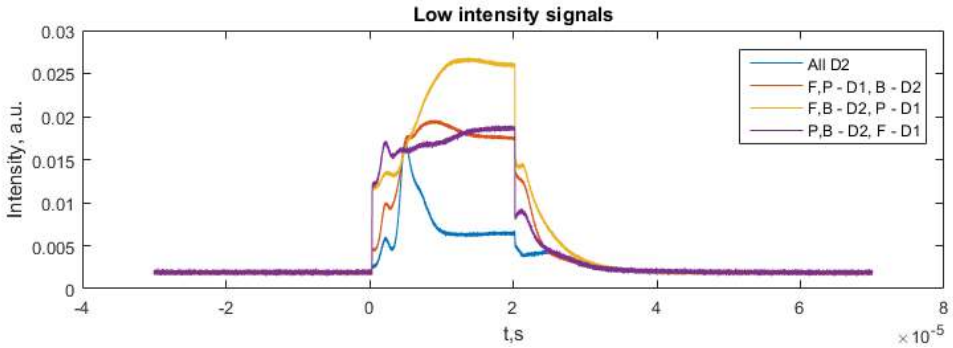

Figure 5.15: Polarization permutations that give weaker signal

Notice that there is also a very weak almost instantaneous signal in respect to t = 0 (start of the incident pulse) in some conjugate pulses. It is most observable in the P,B - D2, F- D1 combination in Figure 5.15. It can be speculated that this signal originates from a $\chi^{(3)}$ process described in Section 2.1, though the amplitude of this signal is rather weak compared to the high-intensity signals in Figure 5.14. This result leans more to conclusions made by Payne *et al.* who argued that the $\chi^{(3)}$ signal is negligible compared to the one from the population grating [22].

After getting the signal curve for the case of D2D2D2 polarization, it is possible to qualitatively compare the signal structure for the two crystals studied in this project (Figure 5.16).

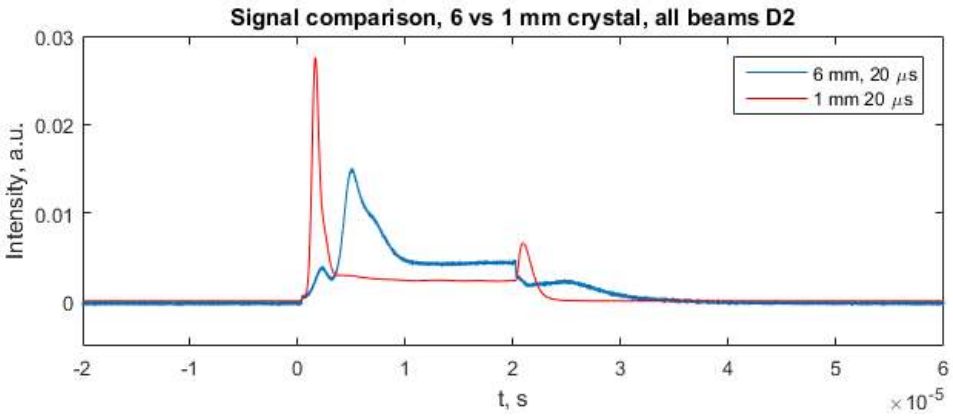

Figure 5.16: Signal structure for 20 µs incoming pulses for 1 and 6-mm-thick crystals with incident beams polarized along D2 axis

The shape of the conjugate signal looks approximately similar for either crystal which indicates a consistent nature of the mechanism for phase conjugation in the Pr:YSO crystal for this particular light polarization. Here, a reasonable explanation for a slower response in the thicker sample could be a slow-light delay discussed earlier.

While performing polarization experiments, it was observed that conjugate signal dynamics (signal buildup and decay) after turning the beams on and off was different for different polarization combinations, and this difference in behaviour was noticeable on a timescale of hundreds of milliseconds. Thus, it was decided to use the mechanical shutter to block and unblock the beams and observe this signal fall and rise dynamics.

Firstly, the shutter was placed in the backward pump and the experimental procedure can be divided into two steps:

1. Send the pulse to the crystal while blocking the B beam (the other two propagate freely)

2. Unblock the shutter and record the sequence of pulses that triggers the oscilloscope

The phase-conjugated signal buildup after the shutter was unblocked is shown in Figure 5.17

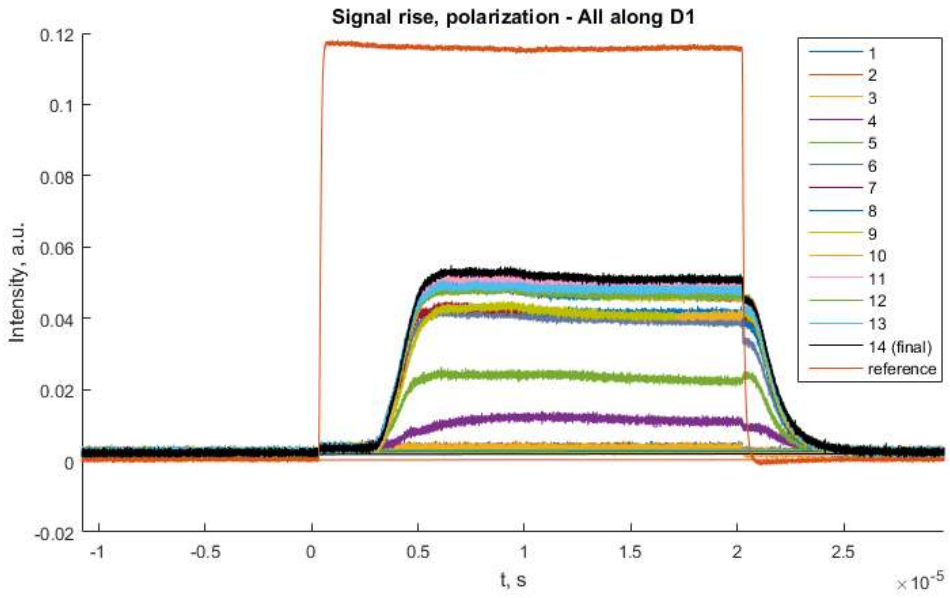

Figure 5.17: Signal rise time sequence when all beams are polarized along D1. Numbers 1-14 on the legend denote respective shots that triggered oscilloscope. Time interval between consecutive shots - 56 ms

It is clear that the signal rises steadily and reaches its stable value approximately 500 ms after the shutter in the backward pump has opened. When the forward pump polarization was changed to be parallel to the D2 axis, after opening the shutter, the signal behaviour was observed to be completely different (Figure 5.18).

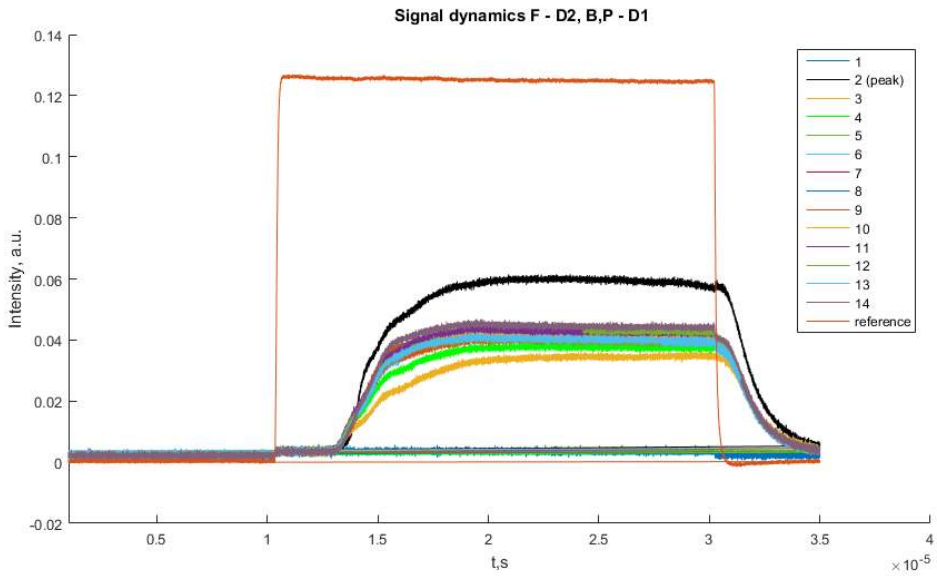

Figure 5.18: Signal rise time with forward pump polarized along D2, rest - D1. Time interval between consecutive shots - 56 ms

Now, the medium responds much quicker and there is even a boost in the signal in one of the first shots (the black "peak" curve). This behaviour was observed consistently with the aforementioned incident pump and probe beam polarizations not having any effect on this peculiarity. It should be noted that while the overall stable signal for this polarization configuration is less efficient (approximately 65-75 % reflectivity), this transient spike in the signal was even stronger (130 % reflectivity) than the D1D1D1 polarization signal (124 % reflectivity).

The reason for such a drastic change in behaviour remains unclear and it is incredibly hard to speculate on what it might be. The first experiment to improve the understanding of this effect would be to flip polarization of the pumps, so that the backward pump was polarized along the D2 and the forward parallel to the D1 axis; this will give an insight if the effect is reciprocal between the pumps, although the signal intensity would be rather low, as was shown before. It would also be interesting to try to slowly vary the polarization state of the F beam, i.e. going from the D2 to the D1 axis and measuring the intensity of this spike. The general conclusion and suggestions for possible future experiments on this matter will be given at the end of this section.

The second step was to place the shutter in the path of the F and P beams simultaneously. In addition to the signal rise dynamics experiment, signal decay after closing the shutter was also observed with a slightly different procedure from the one mentioned above:

1. Send a pulse to the crystal without closing the shutter (All the beams reach the crystal)

2. Close the shutter and send another pulse. Now only the backward pump reaches the crystal and the resulting signal is observed.

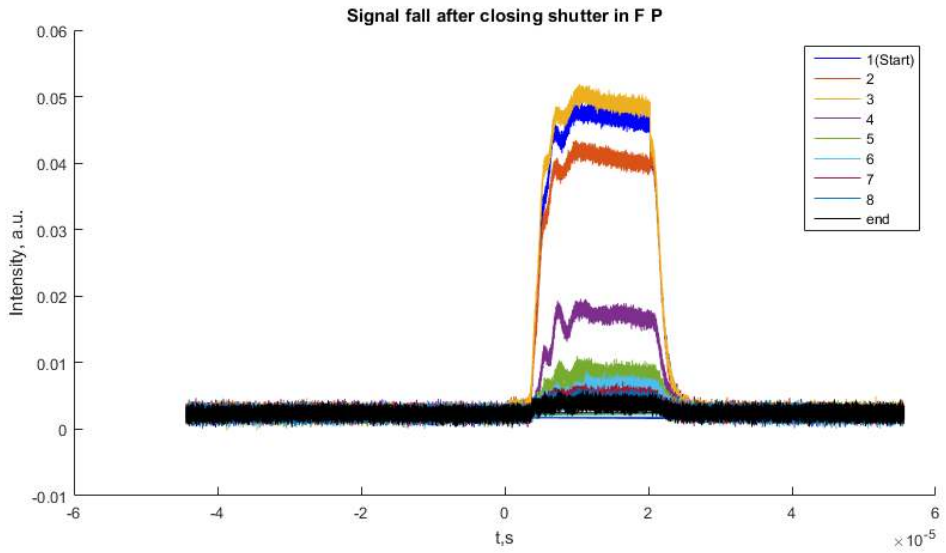

Figure 5.19: Phase-conjugated signal decay dynamics after closing the shutter in the F and P beams. Numbers 1-9 on the legend denote respective shots that triggered oscilloscope Time interval between consecutive shots - 56 ms

It is evident that the signal decays rather slowly - this means that it is most likely a scattering process from the population grating rather than the conventional $\chi^{(3)}$ Four-Wave Mixing process in Kerr-like media. During the first few shots (second and third shots, 56 - 102 ms delay) the signal still possesses most of its strength and then dies out on a timescale of half a second.

Figure 5.20 shows the signal buildup as the shutter unblocks the F and P beams and allows them to propagate through the crystal. The procedure was similar to the one for the backward pump experiment.

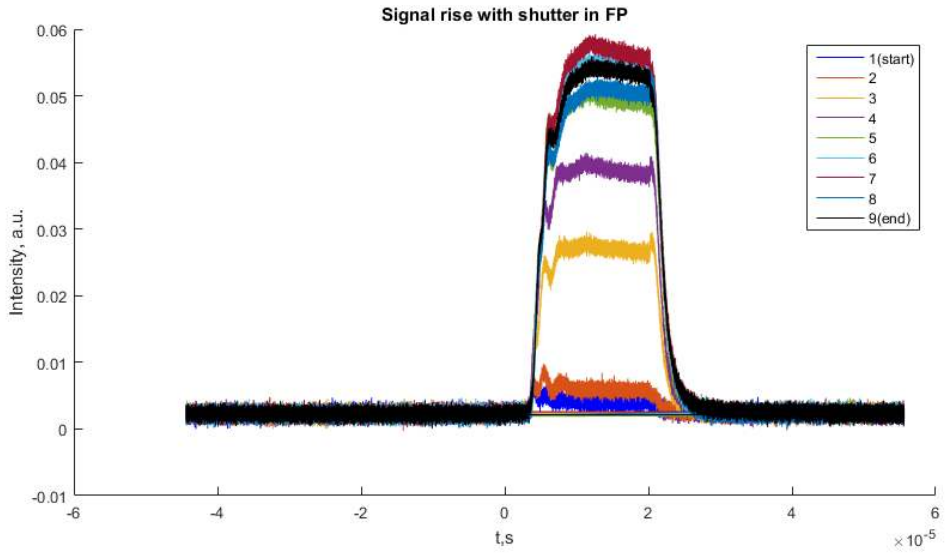

Figure 5.20: Phase-conjugated signal rise dynamics after closing the shutter in the F and P beams

Again, the slow dynamics is clearly observable. This can be explained by the process of building up an effective transmission grating by the F and P beams for

the backward pump to scatter. It was previously mentioned that the main grating which is created could possibly be a population grating between the ground state and the hyperfine metastable state and it usually takes some time to move ions to the metastable state.

To conclude these experiments, it is important to note an overall slow behaviour of the signal. This slow response can also be an indicative of another mechanism for phase conjugation, which was only briefly mentioned in Section 2.2 - a photorefractive effect. This effect can be shortly described as the creation of a static electric field by migration of charges caused by incoming light. This static electric field modulates the index of refraction through an electro-optic (Pockels) effect and thus can also create a grating suitable for scattering either of the beams into the phase-conjugate if the phase matching condition is satisfied. To the author‘s knowledge, it is not very well known if the YSO crystal is strongly or weakly photorefractive. The photorefractive effect is known for being notoriously slow in the low-intensity fields (from seconds up to minutes) [43], and its speed increases with incoming beam intensities. Thus, it is in theory possible to check whether it is the photorefractive phase conjugation or not by measuring the speed of the signal buildup with different optical field amplitudes. Another way to check if this phase conjugation is of photorefractive nature is to vary relative intensities of incoming beams - it is known that the strength of photorefractive effects is at a maximum when all the beam intensities are equal and goes down with a further deviation from this equality [44].

In general, a more advanced experiment would involve the usage of fast electro-optic or acousto-optic modulators in each beam separately which would allow modulating and basically turning the beams on and off on a timescale of nanoseconds. This way, it is not only possible to repeat the experiments above more precisely and with a greater degree of variety, but also to do a time delay measurement, where two of the grating writing beams propagate through the crystal and then are turned off while the third beam is scattered from the recorded structure without the presence of the initial two beams; this measurement will also give a lot of information on the nature of the phase conjugation process in these media. Using the AOMs in particular would also allow us to introduce a separate frequency shift in either of the beams and study the phase conjugation process as a function of detuning from the carrier frequency of the other beams, though one should be careful with using these types of modulators because they alter the transverse mode of the laser beam, so that e.g. an incoming Gaussian mode will not be perfectly Gaussian anymore which in term can affect the spatial overlap between the beams.

The polarization experiments performed for this sample were not done on the 1-mm-thick crystal, so it is of immense interest to do the same measurements on the thin sample. A further outlook on possible future measurements is also given in chapter 6.

5.6 Additional measurements

In the following section a few additional experiments are presented. First, we briefly discuss off-resonant phase conjugation (slow-light effects).

As was shown for the thin crystal, phase conjugation inside of a spectral hole is much less efficient compared to the resonant effect. The same behaviour was observed in the 6-mm-thick crystal. Signal efficiency dropped more than an order of magnitude when propagating inside of the spectral pits of 1 and 17 MHz width. This proves a point that in order to get an efficient phase-conjugated signal it is important to be on resonance, i.e. to have enough ions in the ground state to create the effective population grating for the beams to scatter/reflect from.

The next experiment performed was an investigation of the effect of the frequency shift on the phase-conjugated signal. The detuning affected all three beams with the values ranging from -24 to 24 MHz in respect to the center frequency. The efficiency of the phase-conjugated signal as a function of frequency shift is plotted in Figures 5.21 and 5.22 for the unchirped and chirped signals, respectively.

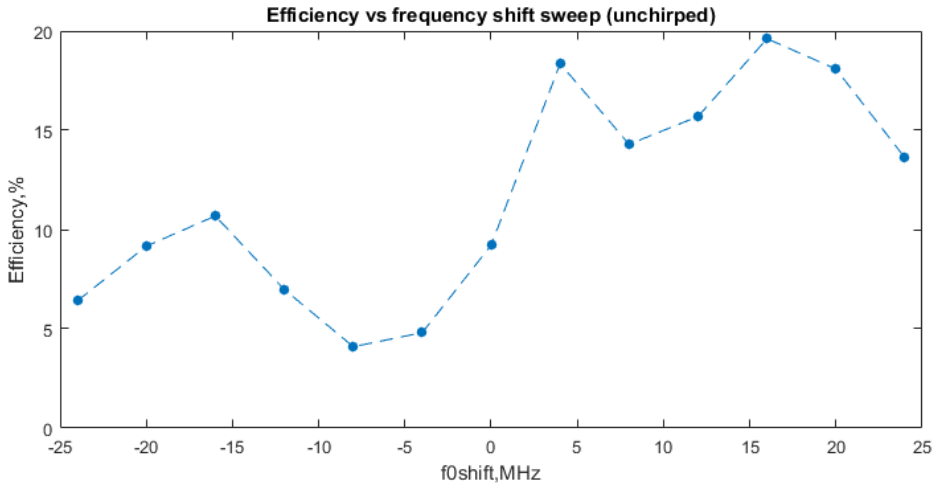

Figure 5.21: Signal efficiency as a function of frequency shift. Unchirped pulse

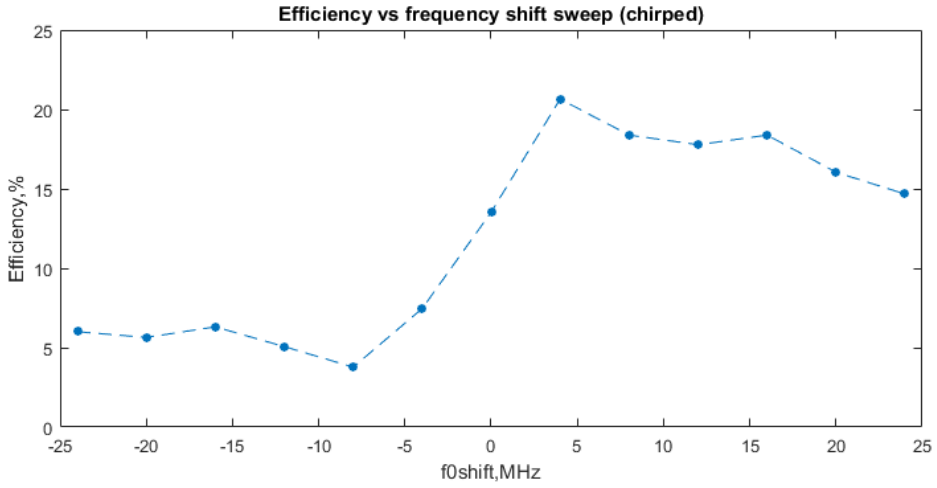

Figure 5.22: Signal efficiency as a function of frequency shift. 1.5 MHz chirped pulse

The difference in the signal efficiency is surprisingly big and it is obvious that the signal with zero shift is not the most efficient one. The general trend is the same for the chirped and unchirped cases, although there are stronger fluctuations in the large shift values in the unchirped curve. The main feature on both plots is the large, almost anti-symmetric change of efficiency in the range approximately from -5 to 5 MHz. In order to illustrate this difference, Figures 5.23 and 5.24 show the signal structure for various frequency shifts.

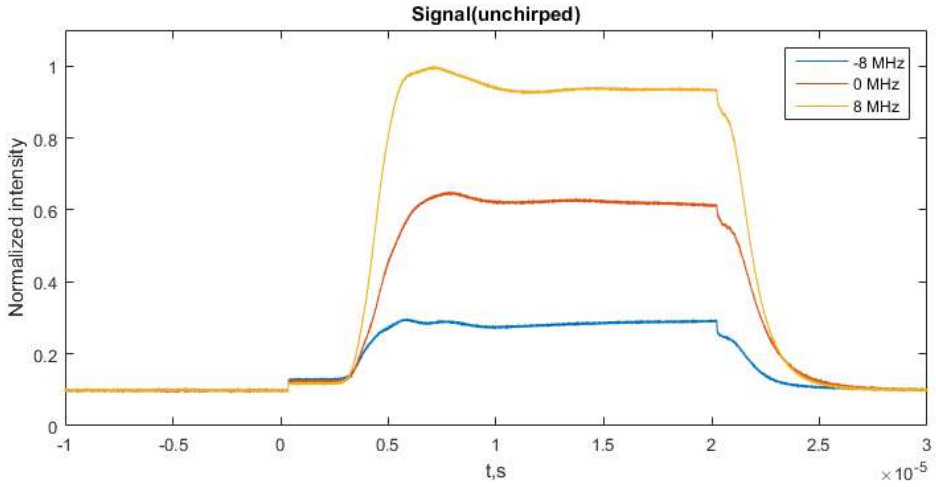

Figure 5.23: Signal structure as a function of frequency shift. Unchirped pulse

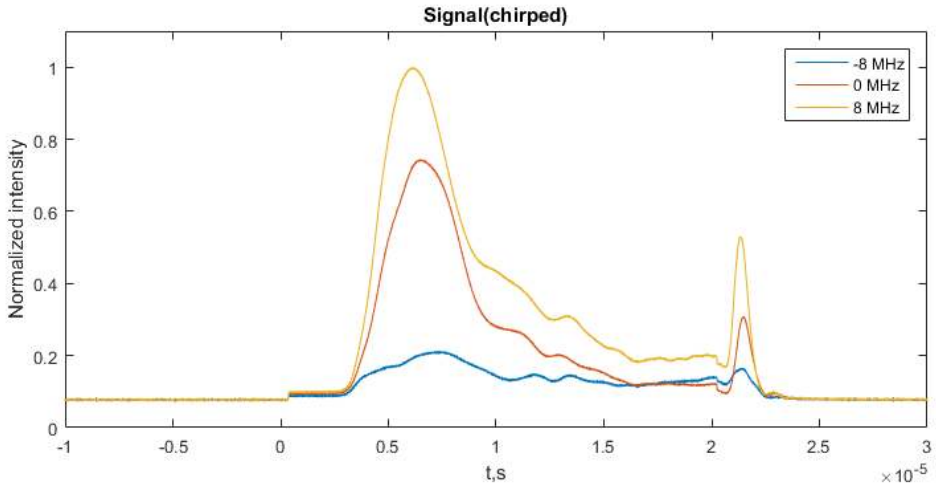

Figure 5.24: Signal structure as a function of frequency shift. 1.5 MHz chirped pulse

Evidently, the +8 Mhz-shifted signal is almost twice as strong as the unshifted one (unchirped case). A similar trend is observed in the other direction, where the 8 MHz-downshifted signal is significantly weaker. The reason for such a behaviour remains unclear, in principle the signal should not change much when the change in frequency is in the range of tens of MHz. This phenomenon can possibly be connected with larger or lower concentration of ions with different resonant frequencies (e.g. the signal is stronger at the frequency f_0+8 MHz because more ions are interacting with this frequency and the resulting population grating is more efficient).

Finally, we discuss how the number of reset pulses affects strength and structure of the phase-conjugated signal. A reset pulse is a broad frequency scanning pulse that is used to restore the initial absorption profile and remove any leftover structures that were created by the conjugate pulse. The actual pulse sequence that was used in the majority of these experiments was:

1. Send the phase-conjugate pulse.
2. Send the reset pulse to restore the absorption profile and remove any spectral holes or unwanted structures.

The signal structure and its efficiency as a function of the number of reset pulses are shown in Figures 5.25 and 5.26.

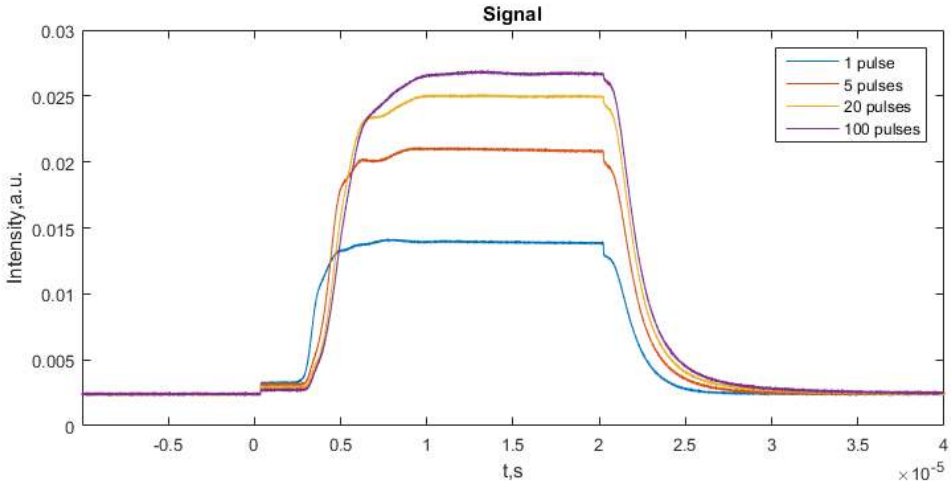

Figure 5.25: Signal structure as a function of quantity of reset pulses

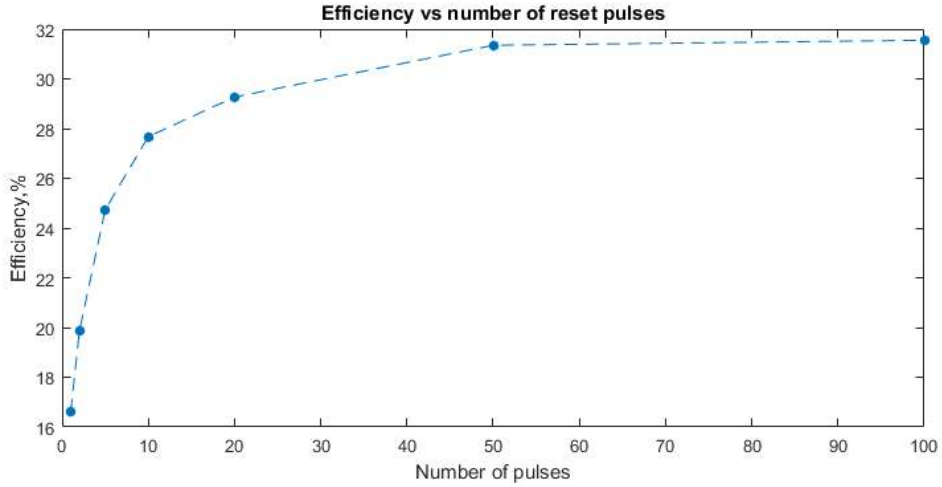

Figure 5.26: Signal efficiency as a function of quantity of reset pulses

From the efficiency curve it is obvious that having less than 20 reset pulses is not enough to effectively move the ions back to the ground state and there are probably some residual spectral pits remaining from the frequency scan phase conjugation pulse. As the number of reset pulses reaches values in the range of 50-100, the signal strength stabilizes, and it most likely means that the initial absorption profile is completely restored and ready for the next phase-conjugating pulse; increasing the number of reset pulses further did not give any increase in the signal at all.

To conclude the findings of this experiment, in future measurements one should choose an optimum amount of reset pulses so that the absorption profile is restored before the next phase-conjugating pulse arrives. An interesting thing to check would be how the signal behaves when one increases or decreases the width of frequency scan of this reset pulse. It is hard to predict what would happen in this case, but most likely there will be no qualitative improvements to the signal as the reset pulse used before was rather broad - 100 MHz wide.

Chapter 6

Conclusions and Outlook

Throughout this project, two experimental sessions were held, and the phase conjugation properties in Praseodymium doped Yttrium Orthosilicate crystals of different thicknesses were studied. The obtained phase-conjugated signal reflectivity in a 1-mm-thick sample was equal to approximately 4 %. Later it was established that the least effective polarization combination was used for the measurements on this thin crystal and reflectivity values up to 124 % were obtained later in the thicker sample. Overall, phase conjugation in the Pr^{3+}:Y_2SiO_5 crystal was studied as a function of pulse duration, laser beam intensity, detuning from resonance, polarization combinations, etc. While large amounts of data were taken, there are still many open questions about the nature and the structure of an OPC process in these media. In this chapter, the author will try to provide some general ideas on possible future experiments which could answer those questions and as well give an outlook and some considerations regarding the implementation of the phase-conjugating elements into the UOT technique.

First, for the 6-mm crystal much more data was taken and more experiments were carried out. It means that in order to adequately compare two samples between each other, it is necessary to do those experiments for the thin crystal as well. Polarization measurements are of particular importance since the largest change in the signal was observed when incoming beam polarization was changed. It would be of great interest to check the signal decay and rise with different light polarization for the thin crystal as well.

The other potentially useful experiment is to investigate optical phase conjugation as a function of spatial beam overlap. This can be done by varying the separation between F and P beams before they hit the lens that guides them to the crystal. It was established that the signal was very sensitive to the optics so getting precise measurements on the beam overlap dependence could provide some insight on how to effectively place and align the optical components when setting up the experiment. Other useful experiments would be a time delay between the pulses and a photorefractive investigation, described previously in Chapter 5.

It is very important to note that while this project describes optical phase conjugation by four-wave mixing, it was not explicitly checked that it was, in fact, the optical phase conjugation, even though it is very unlikely that it is something else. A thorough investigation would involve placing a distorting medium like a piece of glass into the path of the probe and detect a spatial intensity profile of the conjugate wave after passing this distorting medium on the way to the detector:

as was discussed in theory, wavefront distortions should be eliminated. In theory, this is also the next logical step in the further development of this project.

There are still many technical and practical challenges that stand in front of the research team before the OPC is realized in the UOT. In the author‘s opinion, an approximate research plan would go in the following direction:

1. Repeat the measurements that were done for the 6-mm-thick sample on its thinner counterpart and compare the efficiency between the two crystals directly, taking into account beam polarization, the number of reset pulses, etc. Perform the above-suggested experiments and try to further understand the features of phase conjugation in these crystals. Numerical simulations mimicking this effect can potentially be of great help in this regard.

2. Perform the beam distortion experiment described above to confirm whether it is a phase conjugation or not. Study the wave restoration properties of this process. In the meantime, it can possibly be a good idea to research the field for other materials suitable for fast and efficient optical phase conjugation. Ideally, it is important to have the fast phase conjugator (response faster than milliseconds) because drastic changes in living tissue can happen on this timescale and thus can reduce the efficiency of the UOT.

3. If the results are promising for a certain material, perform *in vitro* UOT experiments (e.g. similar to the one described in [35]) involving turbid media e.g. a tissue phantom, and think about the prospects of implementing an external gain medium to amplify the conjugated photons, if required.

4. Further steps would require tackling and overcoming the engineering difficulties (how to effectively place the slow-light filters and phase conjugators in the UOT system) and performing first *in vivo* experiments

The UOT has a great potential as an imaging method and its successful implementation further into the medical industry would be a tremendous achievement for the scientific community, and the author hopes that the usage of phase conjugators in general and findings of this project in particular, will help achieve this goal.

Acknowledgements

First and foremost, I would like to express my gratitude to my supervisors, Stefan Kroll and Qian Li for helping and guiding me throughout this fantastic project. Your help was absolutely invaluable and I am very grateful for the time you devoted to share your experience and knowledge with me. I also would like to thank Adam Kinos who helped me tremendously with practical things in the lab in the later stages of the project. Further, I want to thank Andreas Walther, Lars Rippe, Koray Dincer, Vassily Kornienko and Alexander Bengtsson for a great deal of interesting and useful discussions within the group meetings and during the lunches. I would like to mention my office neighbours Hannes Pahl and Samuel Bengtsson for the cosy environment and interesting friendly conversations. And finally, my eternal love and gratitude go to my parents who supported me through all the highs and lows despite being very far away. All of this would not be possible without you. Your love is my strength.

Bibliography

[1] Q. Peng, A. Juzeniene, J. Chen, L. O. Svaasand, T. Warloe, K-E. Giercksky, and J. Moan. Lasers in medicine. *Reports on Progress in Physics*, 71(5):056701, 2008.

[2] H. Jelínková. 1 - introduction: the history of lasers in medicine. In Helena Jelínková, editor, *Lasers for Medical Applications*, Woodhead Publishing Series in Electronic and Optical Materials, pages 1 – 13. Woodhead Publishing, 2013.

[3] N. Bendsoe and K. Svanberg. 14 - lasers in dermatology. In Helena Jelínková, editor, *Lasers for Medical Applications*, Woodhead Publishing Series in Electronic and Optical Materials, pages 459 – 489. Woodhead Publishing, 2013.

[4] J. D. Carroll, M. R. Milward, P. R. Cooper, M. Hadis, and W.M. Palin. Developments in low level light therapy for dentistry. *Dental Materials*, 30(5):465 – 475, 2014.

[5] A. Douplik, G. Saiko, I. Schelkanova, and V.V. Tuchin. 3 - the response of tissue to laser light. In Helena Jelínková, editor, *Lasers for Medical Applications*, Woodhead Publishing Series in Electronic and Optical Materials, pages 47 – 109. Woodhead Publishing, 2013.

[6] S. Svanberg. 10 - laser spectroscopy in medical diagnostics. In Helena Jelínková, editor, *Lasers for Medical Applications*, Woodhead Publishing Series in Electronic and Optical Materials, pages 286 – 324. Woodhead Publishing, 2013.

[7] Int Commission Non-Ionizing Radiat. ICNIRP guidelines on limits of exposure to laser radiation of wavelengths between 180 nm and 1,000 mu m. *Health Physics*, 105(3):271–295, SEP 2013.

[8] American National Standards Institute and Laser Institute of America. *American National Standard for Safe Use of Lasers.* Laser Institute of America, 2014.

[9] T. Vo-Dinh. *Biomedical photonics handbook.* Boca Raton, Fla. : CRC Press, c2003., 2003.

[10] S. L. Jacques. Optical properties of biological tissues: a review. *Physics in Medicine and Biology*, 58(11):R37, 2013.

[11] A. Yariv and R.A. Fisher. 1 - introduction. In Robert A. Fisher, editor, *Optical Phase Conjunction*, pages 1 – 22. Academic Press, San Diego, 1983.

[12] G. S. He. Optical phase conjugation: principles, techniques, and applications. *Progress in Quantum Electronics*, 26:131–191, May 2002.

[13] B.E.A. Saleh and M.C. Teich. *Fundamentals of Photonics*, pages 894–905. Wiley Series in Pure and Applied Optics. Wiley, 2007.

[14] S. Leveque, A.C. Boccara, M. Lebec, and H. Saint-Jalmes. Ultrasonic tagging of photon paths in scattering media: parallel speckle modulation processing. *Optics Letters*, 24(3):181–183, FEB 1 1999.

[15] H. J. Eichler, P. Günter, and D. W. Pohl. *Laser-Induced Dynamic Gratings*, pages 159–192. Springer Berlin Heidelberg, Berlin, Heidelberg, 1986.

[16] P. R. Hemmer, D. P. Katz, J. Donoghue, M. S. Shahriar, P. Kumar, and M. Cronin-Golomb. Efficient low-intensity optical phase conjugation based on coherent population trapping in sodium. *Opt. Lett.*, 20(9):982–984, May 1995.

[17] M. Y. Lanzerotti, R. W. Schirmer, and A. L. Gaeta. Highreflectivity, widebandwidth optical phase conjugation via fourwave mixing in potassium vapor. *Applied Physics Letters*, 69(9):1199–1201, 1996.

[18] A. Miniewicz, S. Bartkiewicz, and J. Parka. Optical phase conjugation in dye-doped nematic liquid crystal. *Optics Communications*, 149(1-3):89–95, APR 1 1998.

[19] E. Mohajerani, E. Whale, and G.R. Mitchell. Polarisation sensitive optical phase conjugation in novel polymer films. *Optics Communications*, 92(4):403 – 410, 1992.

[20] H. Rajbenbach, J.P. Huignard, and P. Refregier. Amplified phase-conjugate beam reflection by 4-wave mixing with photorefractive Bi12SiO20 crystals. *Optics Letters*, 9(12):558–560, 1984.

[21] P. Günter. Holography, coherent light amplification and optical phase conjugation with photorefractive materials. *Physics Reports*, 93(4):199 – 299, 1982.

[22] R. C. Powell, S. A. Payne, L. L. Chase, and G. D. Wilke. Four-wave mixing of nd^{3+}-doped crystals and glasses. *Phys. Rev. B*, 41:8593–8602, May 1990.

[23] B. S. Ham, P. R. Hemmer, and M. S. Shahriar. Efficient phase conjugation via two-photon coherence in an optically dense crystal. *Phys. Rev. A*, 59:R2583–R2586, Apr 1999.

[24] R.L. Abrams, J.F. Lam, R.C. Lind, D.G. Steel, and P.F. Liao. 8 - phase conjugation and high-resolution spectroscopy by resonant degenerate four-wave mixing. In Robert A. Fisher, editor, *Optical Phase Conjunction*, pages 211 – 284. Academic Press, San Diego, 1983.

[25] Stephen E Harris. Electromagnetically induced transparency. *Physics Today*, 50(7):36–42, 1997.

[26] Elson D. S., R. Li, C. Dunsby, R. Eckersley, and M-X. Tang. Ultrasound-mediated optical tomography: a review of current methods. *Interface Focus*, 1(4):632–648, 2011.

[27] J. Li, G. Ku, and L. V. Wang. Ultrasound-modulated optical tomography of biological tissue by use of contrast of laser speckles. *Appl. Opt.*, 41(28):6030–6035, Oct 2002.

[28] M. Gross, P. Goy, and M. Al-Koussa. Shot-noise detection of ultrasound-tagged photons in ultrasound-modulated optical imaging. *Opt. Lett.*, 28(24):2482–2484, Dec 2003.

[29] J.P. Monchalin, R. Héon, P. Bouchard, and C. Padioleau. Broadband optical detection of ultrasound by optical sideband stripping with a confocal fabry–perot. *Applied Physics Letters*, 55(16):1612–1614, 1989.

[30] B. Jayet, J.-P. Huignard, and F. Ramaz. Optical phase conjugation in nd:yvo4 for acousto-optic detection in scattering media. *Opt. Lett.*, 38(8):1256–1258, Apr 2013.

[31] Y. Li, H. Zhang, C. Kim, K. H. Wagner, P. Hemmer, and L. V. Wang. Pulsed ultrasound-modulated optical tomography using spectral-hole burning as a narrowband spectral filter. *Applied Physics Letters*, 93(1):011111, 2008.

[32] R. N. Shakhmuratov, A. Rebane, P. Mégret, and J. Odeurs. Slow light with persistent hole burning. *Phys. Rev. A*, 71:053811, May 2005.

[33] A. Walther, A. Amari, S. Kröll, and A. Kalachev. Experimental superradiance and slow-light effects for quantum memories. *Phys. Rev. A*, 80:012317, Jul 2009.

[34] Walther A., Rippe L., Wang L.V., Andersson-Engels S., and Kröll S. Is optical imaging of oxygenation at heart depth possible? (manuscript submitted). *Optica*, 2017.

[35] H. Zhang, M. Sabooni, L. Rippe, C. Kim, S. Kröll, L. V. Wang, and P. R. Hemmer. Slow light for deep tissue imaging with ultrasound modulation. *Applied Physics Letters*, 100(13):131102, 2012.

[36] Q. Li, Y. Bao, A. Thuresson, A. N. Nilsson, L. Rippe, and S. Kröll. Slow-light-based optical frequency shifter. *Phys. Rev. A*, 93:043832, Apr 2016.

[37] Y. C. Sun. *Rare Earth Materiais in Optical Storage and Data Processing Applications*, pages 379–429. Springer Berlin Heidelberg, Berlin, Heidelberg, 2005.

[38] A. Walther. *Coherent Processes in Rare-Earth-Ion-Doped Solids*. PhD thesis, Lund University, 2009.

[39] M. Nilsson. *Coherent Interactions in Rare-Earth-Ion-Doped Crystals for Applications in Quantum Information Science*. PhD thesis, Lund University, 2005.

[40] E.D. Black. An introduction to Pound-Drever-Hall laser frequency stabilization. *American Journal of Physics*, 69(1):79–87, JAN 2001.

[41] Wikipedia. Rabi frequency. Link: `wikipedia.org/wiki/Rabi_frequency`.

[42] R.P.M. Green, G.J. Crofts, and M.J. Damzen. Phase conjugate reflectivity and diffraction efficiency of gain gratings in nd:yag. *Optics Communications*, 102(3):288 – 292, 1993.

[43] F. Agulló-López, G. F. Calvo, and M. Carrascosa. *Fundamentals of Photorefractive Phenomena*, pages 43–82. Springer New York, New York, NY, 2006.

[44] J. Feinberg. 11 - optical phase conjugation in photorefractive materials. In Robert A. Fisher, editor, *Optical Phase Conjunction*, pages 417 – 443. Academic Press, San Diego, 1983.